Supplementary Information (SI) for Chemical Science.
This journal is © The Royal Society of Chemistry 2024

Electronic Supplementary Information

Ag(I) emitters with ultrafast spin-flip dynamics for high-efficiency electroluminescence

Ao Ying,‡[a] Nengquan Li,‡[b] Xingyu Chen,[c] Jianlong Xia,[c] Chuluo Yang*[b] and Shaolong Gong*[a]

[a] College of Chemistry and Molecular Sciences, Hubei Key Lab on Organic and Polymeric Optoelectronic Materials, Wuhan University, Wuhan 430072, China

[b] Shenzhen Key Laboratory of New Display and Storage Materials, College of Materials Science and Engineering, Shenzhen University, Shenzhen 518060, China

[c] State Key Laboratory of Advanced Technology for Materials Synthesis and Processing, Center of Smart Materials and Devices, School of Chemistry, Chemical Engineering and Life Science, Wuhan University of Technology, Wuhan 430070, China

* Corresponding Author: slgong@whu.edu.cn (Shaolong Gong); clyang@szu.edu.cn (Chuluo Yang).

‡ These authors contributed equally to this work.

General Information

All reagents were used as received from commercial sources unless otherwise stated. Tetrahydrofuran and toluene were dried by sodium-potassium alloy. ^{1}H NMR,^{13}C NMR and ^{1}H-^{1}H COSY NMR spectra were measured on a Bruker AVANCE III HD 400MHz spectrometer. High-resolution mass spectra (HRMS) were measured on LCQ-Orbitrap Elite (Thermo-Fisher Scientific, Waltham, MA, USA) and 5800MALDITOF (AB SCIEX, Framingham, MA, USA) mass spectrometer. Elemental analysis was performed on Thermo Scientific Flash 2000 elemental analyzer. Cyclic voltammetry (CV) was carried out in nitrogen-purged CH_2Cl_2 at room temperature with a CHI voltammetric analyser. Tetrabutylammonium hexafluorophosphate ($TBAPF_6$) (0.1 M) was used as the supporting electrolyte. The conventional three-electrode configuration consists of a platinum working electrode, a platinum wire auxiliary electrode, and an Ag wire pseudo-reference electrode with ferrocenium–ferrocene (Fc^+/Fc) as the internal standard. Cyclic voltammograms were obtained at a scan rate of 100 mV s^{-1}. Formal potentials are calculated from the half-wave potentials of the oxidation and reduction processes in the CV curves. The HOMO energy levels (eV) of the compounds were calculated according to the formula: -[4.8+($E_{1/2(ox/red)}$-$E_{1/2(Fc/Fc+)}$)] eV. The LUMO energy levels (eV) of the compounds were calculated by using HOMO levels and optical bandgaps. The single crystal was obtained by layering of CH_2Cl_2 solution with n-hexane. The X-ray structural data with collected at 200 K on a Rigaku Oxford Diffraction Supernova Dual Source, Cu at Zero equipped with an AtlasS2 CCD using Cu Kα radiation (λ = 1.54184 Å). Data reduction was carried out with the diffractometer's software.[1] The structures were solved by direct methods using Olex2 software,[2] and the non-hydrogen atoms were located from the trial structure and then refined anisotropically with SHELXL-2018 using a full-matrix least-squares procedure based on F^2.[3] The weighted R factor, wR, and goodness-of-fit S values were obtained based on F^2. The hydrogen atom positions were fixed geometrically at the calculated distances and allowed to ride on their parent atoms. Crystallographic data for the structure reported in this paper have been deposited at the Cambridge

Crystallographic Data Center.[4] Details of the molecules were shown in the table below. Root-mean-square roughness of surface in doped films were measured by a SPM-9700HT atomic force microscope.

Theoretical calculation:

Density functional theory (DFT) and time-dependent DFT (TD-DFT) simulations were performed using Gaussian 16 programs. Ground state structures, potential energies and FMOs were obtained by M06L density functional method with basis set def2-SVP. The dispersion correction was conducted by Grimme's D3 version function.[5,6] Time-dependent DFT (TD-DFT) with M06L functional and basis set def2-SVP were then performed to obtain optimal S_1 structure. The energy levels of S_1 and T_1 were calculated in a theoretical level of PBE0 with def2-SVP. SMD solvent model of CH_2Cl_2 were introduced to simulate the local polar environment. Relativistic effects were conducted during the single-point energy calculation using Douglas-Kroll-Hess 2nd order scalar relativistic calculation. Hole-electron analysis, independent gradient model (IGM) analysis, quantum theory of atoms in molecule (QTAIM) analyses and natural bonding orbital (NBO) analysis were performed using TPSSh functional and def2-SVP basis set and further analysized by Multiwfn 3.8.[7]

Photophysical characterization:

Thin films for photophysical characterization were prepared by spin-coating on 2.0 cm × 1.8 cm quartz substrates using 10 mg mL^{-1} chlorobenzene solutions in a glovebox. All the film samples were encapsulated with UV-curable epoxy. All the solution samples were measured in 1 cm × 1 cm quartz cell. Absorption spectra were characterized by a UV-vis spectrophotometer (UV-2700, Shimadzu). Photoluminescence (PL) and phosphorescence spectra were characterized by a spectrofluorimeter (F-4600, Hitachi Inc.). Absolute photoluminescence quantum efficiencies (Φ_{PL}) of these complexes in dilute solutions or solid state were determined using a Hamamatsu's established C9920-02 measurement system (Hamamatsu Photonics) equipped with a calibrated integrating sphere, a xenon lamp, and a

model C10027-01 photonic multichannel analyzer. During the Φ_{PL} measurements, the integrating sphere was purged with pure and dry nitrogen to keep the environment inert. The selected monochromatic excitation light was used to excite samples placed in the calibrated integrating sphere. All the solution and film samples were measured under N_2 atmosphere. Time-resolved PL (PL decay curves) was measured by monitoring the decay of the intensity at the PL peak wavelength using FluoTime 300 (PicoQuant GmbH) with a Picosecond Pulsed UV-LASTER (LASTER375) (λ_{ex} = 375 nm) as the excitation source. No light filter was used. For temperature-dependent TRPL measurements, the samples were placed in a vacuum cryostat chamber with temperature control while the other conditions were kept the same. The solution samples were prepared in a glovebox and sealed for TRPL measurement.

Femtosecond transient absorption (fs-TA) spectroscopy:

Fs-TA was performed using a commercial femtosecond pump–probe system (Transient Absorption Spectrometer, Newport Corporation). A laser pulse at 1040 nm with < 400 fs duration is used as a seed to generate a 200 kHz output through a regenerative amplifier in the laser system (Spirit 1040-8-SHG, Newport Corporation). The probe beam is a white light continuum beam spanning from 500 nm to 1000 nm, created by focusing a fraction of the 1040 nm fundamental output onto a YAG crystal. The pump pulse with single wavelength comes from the rest of the output transferred by a TOPAS optical parametric amplifier. The pump−probe delay is controlled by a mechanical delay stage. The samples were dissolved in chlorobenzene with a quartz cuvette (2 mm path length).

Nanosecond transient absorption (ns-TA) spectroscopy:

A commercial sub-nanosecond transient spectrometer (Helios-EOS Fire, Ultrafast System Corporation) was used to perform the excited states' dynamics on a ns-µs time scale. The matched laser system can produce a white light continuum with a range of 350-900 nm as the probe pulse. The delay time is

transformed by electronic control and it has a time window of 1 ns~400 μs. The pump pulse originates from the same source of fs-TA. In order to eliminate the influence of the oxygen molecules dissolved, a pretreatment of degassing with N_2 gas for 10 minutes was required for the samples.

Device fabrication and measurement:

The fabricated devices were based on the structures of ITO/PEDOT:PSS (35 nm)/mCP: 30 wt% Ag(I) emitter (40 nm)/PPF (10 nm)/TmPyPB (50 nm)/LiF (1 nm)/Al (100 nm). The indium tin oxide (ITO) substrate was first subjected to ultrasonic treatment in ethyl alcohol, deionized water, acetone, and ethyl alcohol for 50 minutes. It was then dried at 120 °C for 5 minutes and treated with plasma for 12 minutes. A layer of PEDOT:PSS was spin-coated onto the pre-cleaned ITO and annealed at 120 °C for 30 minutes under ambient conditions. Subsequently, the devices were transferred into a nitrogen-filled glovebox to prepare the corresponding emissive layer. The Ag(I) complexes were dissolved in fresh chlorobenzene solvent at a concentration of 10 mg/mL. The respect solutions were stirred at 50 °C for approximately 30 minutes before spin-coating them to form a ca. 40 nm-thick emissive layer. The devices were then annealed at 100 °C for 10 minutes. Following this, the layers of PPF (10 nm)/TmPyPB (50 nm)/LiF (1 nm)/Al (100 nm) were sequentially fabricated in a vacuum chamber with a base pressure less than 4×10^{-4} Pa. The emitting area of the OLED device was 0.09 cm^2. The *J–L–V* characteristics, EL spectra and EQEs were measured by a Keithley source measurement unit (Keithley 2400) and an absolute EQE measurement system (C9920-12, Hamamatsu Photonics, Japan). All measurements were carried out at room temperature under ambient conditions.

Temperature-dependent lifetime analysis

The temperature-dependent lifetimes were analyzed according to the literature methods.[7] The two-level Boltzmann-type equation is presented in Eq. S1, where $k_{r,S}$ and $k_{r,T}$ is the radiative constant of lowest singlet and triplet states, respectively, k_B is the Boltzmann's constant, T is the temperature.

$$\tau = \frac{3+\exp\left(-\frac{\Delta E_{\mathrm{ST}}}{k_{\mathrm{B}}T}\right)}{k_{r,s}+3k_{r,T}\exp\left(-\frac{\Delta E_{\mathrm{ST}}}{k_{\mathrm{B}}T}\right)} \qquad \text{(S1)}$$

For TADF emitters, the logarithm of radiative constant (k_{d}) shows a linear dependence with respect to 1/T, which can be fitted to Arrhenius equation (Eq. S2) as follows:

$$ln\,(k_{\mathrm{d}}) = ln\left(\frac{k_{\mathrm{ISC}}}{3}\left(1-\frac{k_{\mathrm{ISC}}}{k_{\mathrm{r,S}}+k_{\mathrm{nr,S}}+k_{\mathrm{ISC}}}\right)\right) - \frac{\Delta E_{\mathrm{ST}}}{k_{\mathrm{B}}T} \qquad \text{(S2)}$$

Where k_{ISC} is the rate constant of intersystem constant, $k_{\mathrm{nr,s}}$ is the nonradiative constant of singlet.

Estimation of experimental oscillator strengths:

The theoretical quantity of the oscillator strength f in the classical theory of light absorption is related to the extinction coefficient ε of absorption by the eqution (Eq. S3) as follows:

$$f \equiv 4.3\times10^{-9}\int \varepsilon\, d\,\bar{\nu} \approx\ 4.3\times10^{-9}\varepsilon_{max}\Delta\bar{\nu} \qquad \text{(S3)}$$

Where ε is the experimental extinction coefficient and $\bar{\nu}$ is the energy of the absorption. With the assumption that the absorption spectrum is a smooth Gaussian curve which can be approximated by an isosceles triangle, we can have $\int \varepsilon\, d\,\bar{\nu}\ \approx\ \varepsilon_{max}\Delta\bar{\nu}$, where $\varepsilon_{\mathrm{max}}$ is the value of ε at the absorption maximum and $\Delta\bar{\nu}$ is the full-width half-maximum (FWHM) of the absorption band.

Synthesis of the complexes:

All reagents were used as received from commercial sources unless otherwise stated. The key carbene-silver precursor (MAC)AgCl was synthesized according to the reported procedures in the literature.[8] The key amide ligand 12*H*-benzo[4,5]thieno[2,3-*a*]carbazole (12BT) were purchased from commercial sources.

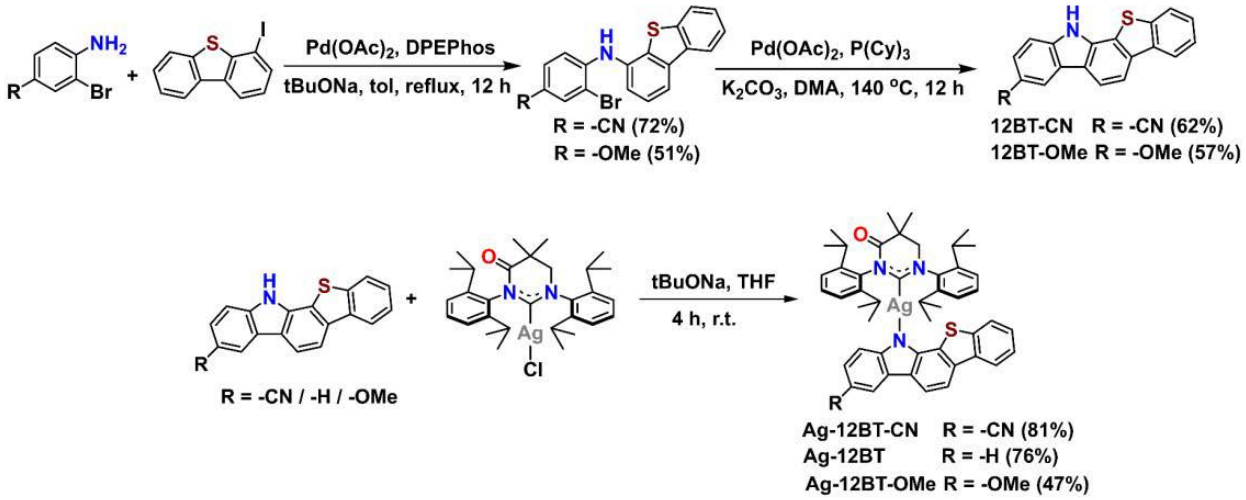

Scheme S1. Synthetic route of Ag-12BT-CN, Ag-12BT, and Ag-12BT-OMe.

Synthesis of DBTNHBr-CN

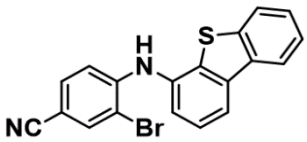

The mixture of 4-amino-3-bromobenzonitrile (1.59 g, 8.1 mmol), 4-iododibenzo[b,d]thiophene (3.00 g, 9.7 mmol), $Pd(OAc)_2$ (0.054 g, 0.24 mmol), bis(2-diphenylphosphinophenyl)ether (0.392 g, 0.72 mmol) and tBuONa (0.775 g, 8.1 mmol) in dry toluene (50 mL) was stirred at reflux overnight and then cooled to room temperature. The reaction mixture was extracted with CH_2Cl_2 (100 mL × 3). The organic phase was dried over anhydrous Na_2SO_4, filtered, and concentrated under reduced pressure. The crude product was purified by column chromatography with petroleum ether/CH_2Cl_2 (v/v = 1/3) as the eluent to afford the white powder (2.21 g, 5.8 mmol). Yield: 72%. ^{1}H NMR (400 MHz, $CDCl_3$ + TMS, 300 K) δ (ppm) 8.22 – 8.15 (m, 1H), 8.09 (d, *J* = 7.9 Hz, 1H), 7.88 – 7.79 (m, 2H), 7.57 – 7.46 (m, 3H), 7.41 (d, *J* = 7.7 Hz, 1H), 7.35 (dd, *J* = 8.6, 1.9 Hz, 1H), 6.77 (d, *J* = 8.6 Hz, 1H), 6.65 (br, 1H). ^{13}C NMR (101 MHz, $CDCl_3$, 300 K) δ (ppm) 145.6, 138.9, 137. 8, 136.4, 136.3, 135.8, 133.5, 132.4, 127.4, 125.8, 124.9, 123.0, 122.8, 122.0, 119.7, 118.4, 113.8, 109.7, 102.4.

Synthesis of DBTNHBr-OMe

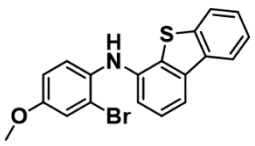

The mixture of 2-bromo-4-methoxyaniline (1.96 g, 9.7 mmol), 4-iododibenzo[b,d]thiophene (3.00 g, 9.7 mmol), $Pd(OAc)_2$ (0.065 g, 0.30 mmol), bis(2-diphenylphosphinophenyl)ether (0.470 g, 0.87 mmol) and tBuONa (0.929 g, 9.7 mmol) in dry toluene (50 mL) was stirred at reflux overnight and then cooled to room temperature. The reaction mixture was extracted with CH_2Cl_2 (100 mL × 3). The organic phase was dried over anhydrous Na_2SO_4, filtered, and concentrated under reduced pressure. The crude product was purified by column chromatography with petroleum ether/CH_2Cl_2 (v/v = 4/1) as the eluent to afford the colorless oil (1.86 g, 4.9 mmol). Yield: 51%. ^{1}H NMR (400 MHz, $CDCl_3$ + TMS, 300 K) δ (ppm) ^{1}H NMR (400 MHz, Chloroform-*d*) δ 8.19 – 8.10 (m, 1H), 7.90 – 7.78 (m, 2H), 7.51 – 7.42 (m, 2H), 7.38 (t, *J* = 7.8 Hz, 1H), 7.22 – 7.08 (m, 3H), 6.81 (dd, *J* = 8.9, 2.8 Hz, 1H), 5.79 (br, 1H), 3.79 (s, 3H). ^{13}C NMR (101 MHz, $CDCl_3$, 300 K) δ (ppm) 154.9, 138.9, 138.4, 137.2, 136.3, 134.2, 131.0, 126.9, 125.6, 124. 6, 123.0, 121.9, 120.7, 118.4, 115. 6, 115.5, 115.0, 114.4, 55.9.

Synthesis of 12BT-CN

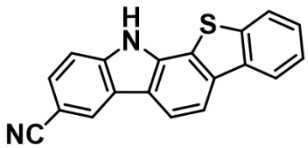

The mixture of DBTNHBr-CN (2.361 g, 6.2 mmol), tricyclohexylphosphane (1.052 g, 3.8 mmol), K_2CO_3 (1.725 g, 12.5 mmol), and $Pd(OAc)_2$ (0.421 g, 1.9 mmol) in dry dimethylacetamide (35 mL) was stirred at 140 ^{o}C for 12 h and then cooled to room temperature. The reaction mixture was poured into 500 mL ice water and then filtered. The solid was washed for three times with 50 mL toluene, CH_2Cl_2 and THF, respectively. The crude product was further purified by vacuum sublimation at 200 ^{o}C, 1×10^{-4} Pa to afford white powder (1.15 g, 3.8 mmol). Yield: 62%. ^{1}H NMR (400 MHz, DMSO-d_6, 300 K) δ (ppm) 12.63 (br, 1H), 8.82 (s, 1H), 8.46 (d, *J* = 9.2 Hz, 1H), 8.38 (d, *J* = 8.2 Hz, 1H), 8.27 (d, *J* = 8.4 Hz, 1H), 8.20 – 8.12 (m, 1H), 7.81 (dd, *J* = 8.4, 1.6 Hz, 1H), 7.73 (d, *J* = 8.4 Hz, 1H), 7.61 – 7.50 (m, 2H). ^{13}C NMR (101 MHz, DMSO-d_6, 300 K) δ (ppm)

142.1, 138. 9, 136.4, 135.4, 135.0, 128.9, 127.2, 126.2, 125.5, 123.9, 123.7, 122.7, 121.8, 120.9, 120.5, 118.5, 114.8, 113.0, 101.6. HRMS (ESI, *m/z*) $[M+H]^+$ calcd. For $C_{19}H_{11}N_2S^+$ 299.0638, found 299.0638.

Synthesis of 12BT-OMe

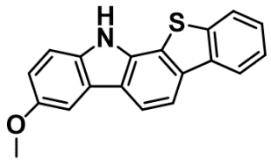

The mixture of DBTNHBr-OMe (3.159 g, 8.2 mmol), tricyclohexylphosphane (1.380 g, 4.9 mmol), K_2CO_3 (2.270 g, 16.4 mmol), and $Pd(OAc)_2$ (0.554 g, 2.5 mmol) in dry dimethylacetamide (40 mL) was stirred at 140 ℃ for 12 h and then cooled to room temperature. The reaction mixture was poured into 500 mL ice water and then filtered. The reaction mixture was extracted with CH_2Cl_2 (100 mL × 3). The organic phase was dried over anhydrous Na_2SO_4, filtered, and concentrated under reduced pressure. The crude product was purified by column chromatography with petroleum ether/CH_2Cl_2 (v/v = 2/1) as the eluent to afford the white powder (1.48 g, 4.7 mmol). Yield: 57%. ^{1}H NMR (400 MHz, DMSO-d_6, 300 K) δ (ppm) 11.80 (br, 1H), 8.40 (d, *J* = 7.1 Hz, 1H), 8.25 (d, *J* = 8.3 Hz, 1H), 8.12 (d, *J* = 4.3 Hz, 2H), 7.96 (s, 1H), 7.78 (d, *J* = 2.5 Hz, 1H), 7.52 (dd, *J* = 17.6, 8.9 Hz, 3H), 7.08 (dd, *J* = 8.8, 2.5 Hz, 1H), 3.89 (s, 3H). ^{13}C NMR (101 MHz, DMSO-d_6, 300 K) δ (ppm) 162.8, 154.0, 138.6, 136. 8, 135.2, 135.0, 133.7, 126.7, 125.3, 123.9, 123.8, 122.4, 121.4, 121.2, 118.1, 115.5, 113.0, 112.6, 103. 3, 56.1. HRMS (ESI, *m/z*) $[M+H]^+$ calcd. For $C_{14}H_{10}NOS^+$ 208.0757, found 208.0756.

Synthesis of Ag-12BT-CN

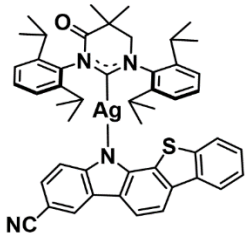

The 12BT-CN ligand (200 mg, 0.73 mmol) and NaH (21 mg, 0.88 mmol) were dissolved in 25 mL THF and stirred for 0.5 h at 50 °C. (MAC)AgCl (431 mg, 0.73 mmol) was added to the reaction mixture and stirred for 4 h. The resulting mixture was filtered through Celite, and the solvent was removed under reduced pressure to afford a white solid. The solid was further redissolved in dry THF and filtered through

microporus filter. The solvent was removed under reduced pressure. The corresponding solid were dissolved in dry CH_2Cl_2 and dry *n*-hexane was added to precipitate the desired crystalline product (504 mg, 0.59 mmol). Yield: 81%. ^{1}H NMR (400 MHz, CD_2Cl_2, 300 K) δ (ppm) 8.16 (s, 1H, C**H**^{4}(Cz)), 8.09 – 8.04 (m, 1H, C**H**^{4}(benzothiophene)), 7.92 (d, *J* = 8.2 Hz, 1H, C**H**^{4}(Cz)), 7.90 – 7.85 (m, 1H, C**H**^{1}(benzothiophene)), 7.76 – 7.63 (m, 3H, C**H**^{3}(Cz) & *p*-Ar**H**), 7.43 (t, *J* = 8.2 Hz, 4H, *m*-Ar**H**), 7.40 – 7.33 (m, 2H, C**H**^{2,3}(benzothiophene)), 7.13 – 7.10 (m, 1H, C**H**^{2}(Cz)), 5.47 (s, 1H, C**H**^{1}(Cz)), 3.89 (s, 2H, CC**H**$_2$N), 3.30 (hept, *J* = 6.7 Hz, 2H, C**H**(CH_3)$_2$), 3.05 (hept, *J* = 6.8 Hz, 2H, C**H**(CH_3)$_2$), 1.54 (s, 6H, C(C**H**$_3$)$_2$), 1.36 (d, *J* = 6.9 Hz, 6H, CH(C**H**$_3$)$_2$), 1.28 (d, *J* = 6.8 Hz, 6H, CH(C**H**$_3$)$_2$), 1.22 (d, *J* = 6.8 Hz, 6H, CH(C**H**$_3$)$_2$), 1.18 (d, *J* = 6.8 Hz, 6H, CH(C**H**$_3$)$_2$).^{13}C NMR (101 MHz, CD_2Cl_2, 300 K) δ (ppm) 217.0, 214.9, 170.9, 146.3, 144.9, 141.4, 139.1, 137.5, 136.9, 130.9, 130.6, 126.1, 125.2, 124.3, 124.2, 122.8, 121.4, 121.2, 116.9, 115.7, 110.8, 62.4, 37.9, 29.2, 28.8, 25.1, 24.4, 24.2, 24.1, 23.8. HRMS (ESI, m/z) $[M]^+$ for $C_{49}H_{52}AgN_4OS^+$ 851.2907, found 851.2906. Elemental analysis calcd for $C_{49}H_{51}AgN_4OS$ (%): C 69.00, H 6.15, N 6.57, S 3.76; found: C 68.5, H 6.16, N 6.60, S 3.76.

Synthesis of Ag-12BT

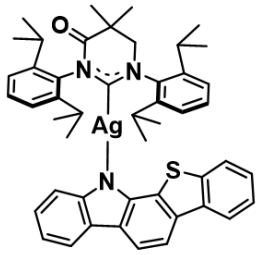

The 12BT ligand (200 mg, 0.80 mmol) and NaH (23 mg, 0.96 mmol) were dissolved in 25 mL THF and stirred for 0.5 h at 50 °C. (MAC)AgCl (474 mg, 0.80 mmol) was added to the reaction mixture and stirred for 4 h. The resulting mixture was filtered through Celite, and the solvent was removed under reduced pressure to afford a white solid. The solid was further redissolved in dry THF and filtered through microporus filter. The solvent was removed under reduced pressure. The corresponding solid were dissolved in dry CH_2Cl_2 and dry *n*-hexane was added to precipitate the desired crystalline product (497 mg, 0.60 mmol). Yield: 75%. ^{1}H NMR (400 MHz, Acetone-d_6, 300 K) δ (ppm) 8.16 (d, *J* = 9.2 Hz, 1H, C**H**^{4}(benzothiophene)), 8.08 (d, *J* = 9.1 Hz, 1H, C**H**^{1}(benzothiophene)), 7.95 (d, *J* = 8.1 Hz, 1H, C**H**^{4}(Cz)), 7.86 (d, *J* = 7.6 Hz, 1H, C**H**^{4}(Cz)), 7.83 – 7.72 (m, 2H, *p*-Ar**H**), 7.68 (d, *J* = 8.1 Hz, 1H, C**H**^{3}(Cz)), 7.64 (d, *J* =

7.8 Hz, 2H, *m*-Ar**H**), 7.56 (d, *J* = 7.8 Hz, 2H, *m*-Ar**H**), 7.41 (dd, *J* = 6.0, 3.2 Hz, 2H, C**H**^{2,3}(benzothiophene)), 6.96 – 6.89 (t, *J* = 7.2 Hz, 1H, C**H**^{2}(Cz)), 6.84 (t, *J* = 7.3 Hz, 1H, C**H**^{3}(Cz)), 5.70 (d, *J* = 8.1 Hz, 1H, C**H**^{1}(Cz)), 4.34 (s, 2H, CC**H**$_2$N), 3.61 (hept, *J* = 6.7 Hz, 2H, C**H**$(CH_3)_2$), 3.36 (hept, *J* = 6.8 Hz, 2H, C**H**$(CH_3)_2$), 1.68 (s, 6H, C(C**H**$_3)_2$), 1.46 (d, *J* = 6.8 Hz, 6H, CH(C**H**$_3)_2$), 1.41 (d, *J* = 6.8 Hz, 6H, CH(C**H**$_3)_2$), 1.35 (d, *J* = 6.9 Hz, 6H, CH(C**H**$_3)_2$), 1.26 (d, *J* = 6.8 Hz, 6H, CH(C**H**$_3)_2$).^{13}C NMR (101 MHz, CD_2Cl_2, 300 K) δ (ppm) 217.9, 215.7, 171.1, 146.3, 144.9, 141.5, 139.1, 137.1, 130.9, 130.7, 126.2, 125.3, 124.7, 124.3, 124.0, 122.8, 121.9, 121.2, 118.9, 116.9, 116.0, 115.5, 108.9, 62.4, 38.0, 29.3, 29.0, 25.2, 24.5, 24.4, 24.2, 24.0. HRMS (ESI, m/z) $[M+H]^+$ calcd for $C_{48}H_{52}AgN_3OS^+$ 826.2955, found 826.2947. Elemental analysis calcd for $C_{48}H_{51}AgN_4OS$ (%): C 72.05, H 7.00, N 5.73, S 4.37; found: C 71.94, H 7.02, N 5.63, S 4.42.

Synthesis of Ag-12BT-OMe

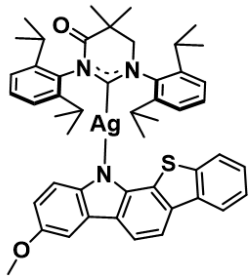

The 12BT-OMe ligand (260 mg, 0.93 mmol) and NaH (27 mg, 1.11 mmol) were dissolved in 25 mL THF and stirred for 0.5 h at 50 °C. (MAC)AgCl (500 mg, 0.93 mmol) was added to the reaction mixture and stirred for 4 h. The resulting mixture was filtered through Celite, and the solvent was removed under reduced pressure to afford a white solid. The solid was further redissolved in dry THF and filtered through microporus filter. The solvent was removed under reduced pressure. The corresponding solid were dissolved in dry CH_2Cl_2 and dry *n*-hexane was added to precipitate the desired crystalline product (341 mg, 0.40 mmol). Yield: 47%. ^{1}H NMR (400 MHz, CD_2Cl_2, 300 K) δ (ppm) 8.04 – 7.98 (m, 1H, C**H**^{4}(benzothiophene)), 7.86 – 7.82 (m, 2H, C**H**^{4}(Cz)), 7.71 – 7.61 (m, 2H, *p*-Ar**H**), 7.52 (d, *J* = 8.1 Hz, 1H, C**H**^{3}(Cz)), 7.42 (t, *J* = 8.0 Hz, 4H, *m*-Ar**H**), 7.36 – 7.27 (m, 3H, C**H**$^{1-3}$(benzothiophene)), 6.51 (dd, *J* = 8.7, 2.6 Hz, 1H, C**H**^{2}(Cz)), 5.36 (d, *J* = 8.7 Hz, 1H, C**H**^{1}(Cz)), 3.87 (s, 2H, CC**H**$_2$N), 3.77 (s, 3H, OC**H**$_3$), 3.31 (hept, *J* = 6.8 Hz, 2H, C**H**$(CH_3)_3$), 3.06 (hept, *J* = 6.8 Hz, 2H, C**H**$(CH_3)_3$), 1.53 (s, 6H, C (C**H**$_3)_2$), 1.35 (d, *J* = 6.9 Hz, 6H, CH(C**H**$_3)_3$), 1.30 (d, *J* = 6.8 Hz, 6H, CH(C**H**$_3)_3$), 1.25 – 1.17 (d, *J* = 6.9 Hz, 12H).^{13}C NMR (101 MHz, CD_2Cl_2, 300 K) δ (ppm) 217.9, 215.5, 171.1, 152.1, 146.4, 145.5, 144.9, 144.6, 141.5, 139.0, 138.2, 136. 6, 131.1,

130.9, 130.7, 126.2, 125.3, 124.6, 124.0, 122.8, 121.1, 116.8, 116.2, 112.9, 108. 5, 100. 9, 62.5, 56.0, 38.0, 31.7, 30.7, 29.3, 29.0, 25.2, 24.5, 24.4, 24.3, 24.0, 22.8. HRMS (ESI, m/z) $[M+H]^+$ for $C_{49}H_{55}AgN_3O_2S^+$ 856.3060, found 856.3057. Elemental analysis calcd for $C_{49}H_{54}AgN_3O_2S$ (%): C 68.60, H 6.46, N 4.90, S 3.74; found: C 68.22, H 6.66, N 4.59, S 3.74.

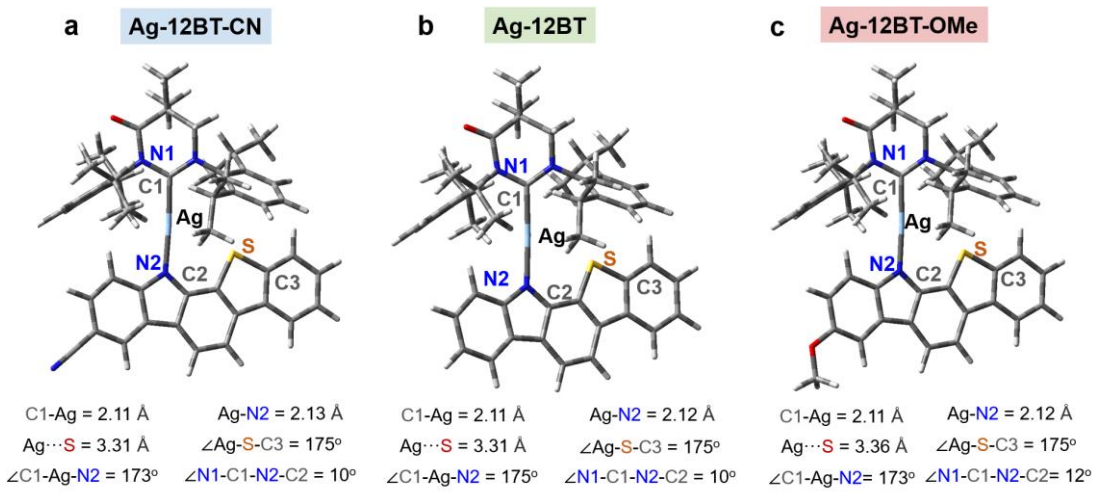

Fig. S1 Optimized S_0 structures of (a) Ag-12BT-CN, (b) Ag-12BT, and (c) Ag-12BT-OMe.

Table S1. Excited state properties of Ag(I) emitters

	Ag-12BT-CN	Ag-12BT	Ag-12BT-OMe
S_1 electron	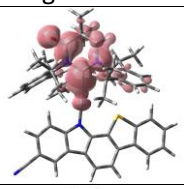	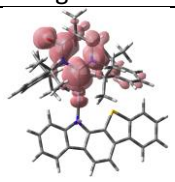	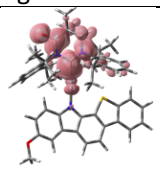
S_1 hole		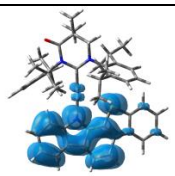	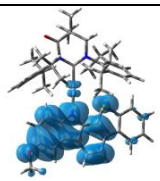
$\Delta Ag\%-S_1$	2.3%	2.6%	2.6%
T_1 hole	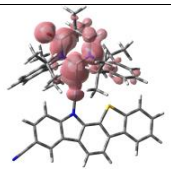	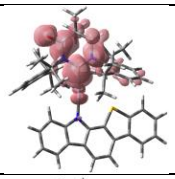	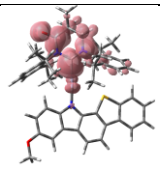
T_1 electron	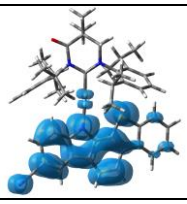	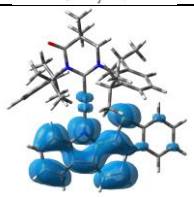	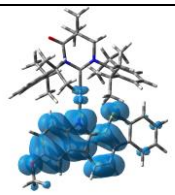
$\Delta Ag\%-T_1$	3.8%	3.5%	3.8%
$SOC<S_1,T_1>$	0.060207	1.53204	1.60351

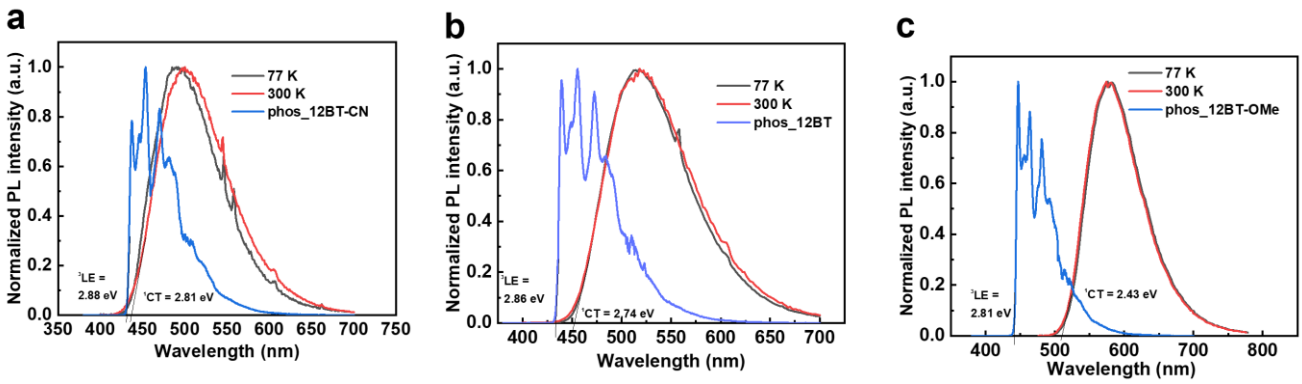

Fig. S2 Comparison of normalized PL spectra of Ag(I) emitters at 77 K and 300 K with phosphorescence spectra from local triplet excited states of the respective amide ligands, following excitation at 375 nm.

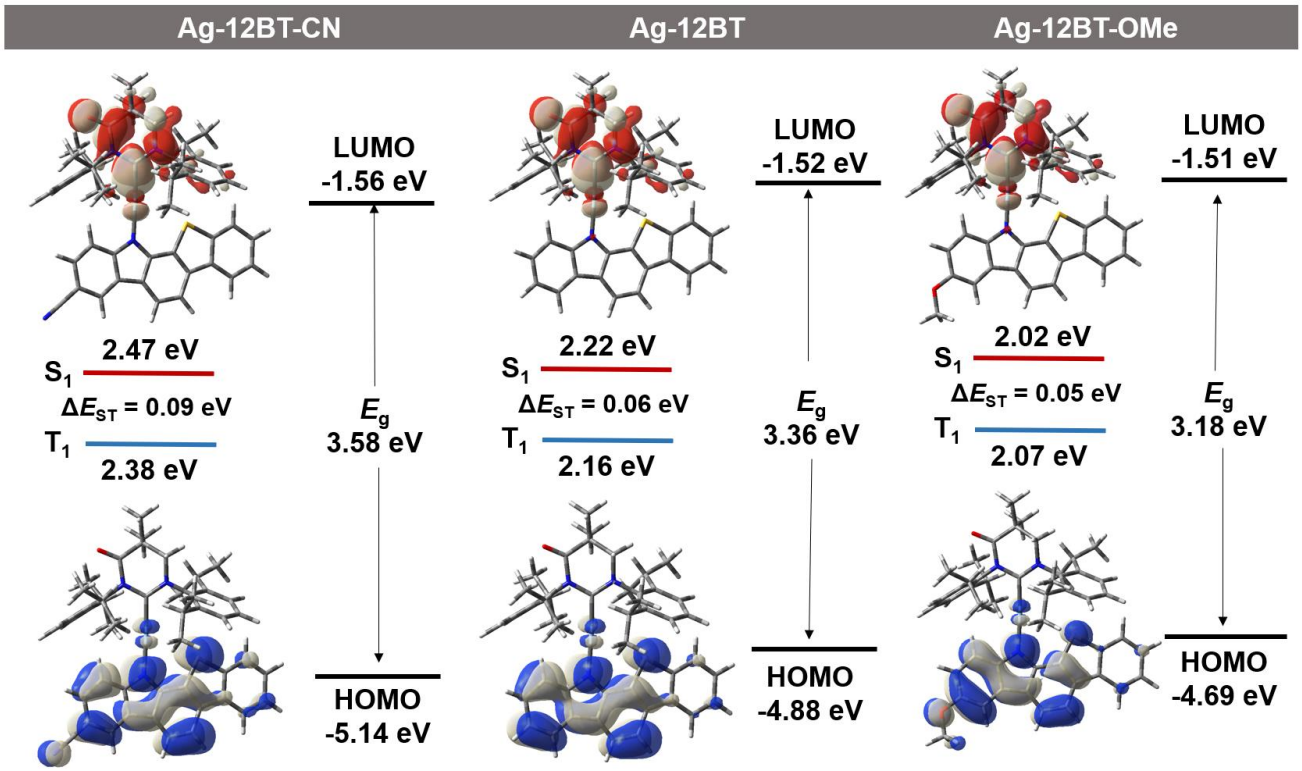

Fig. S3 Calculated energy levels and frontier molecular orbital distributions of Ag-12BT-CN, Ag-12BT, and Ag-12BT-OMe.

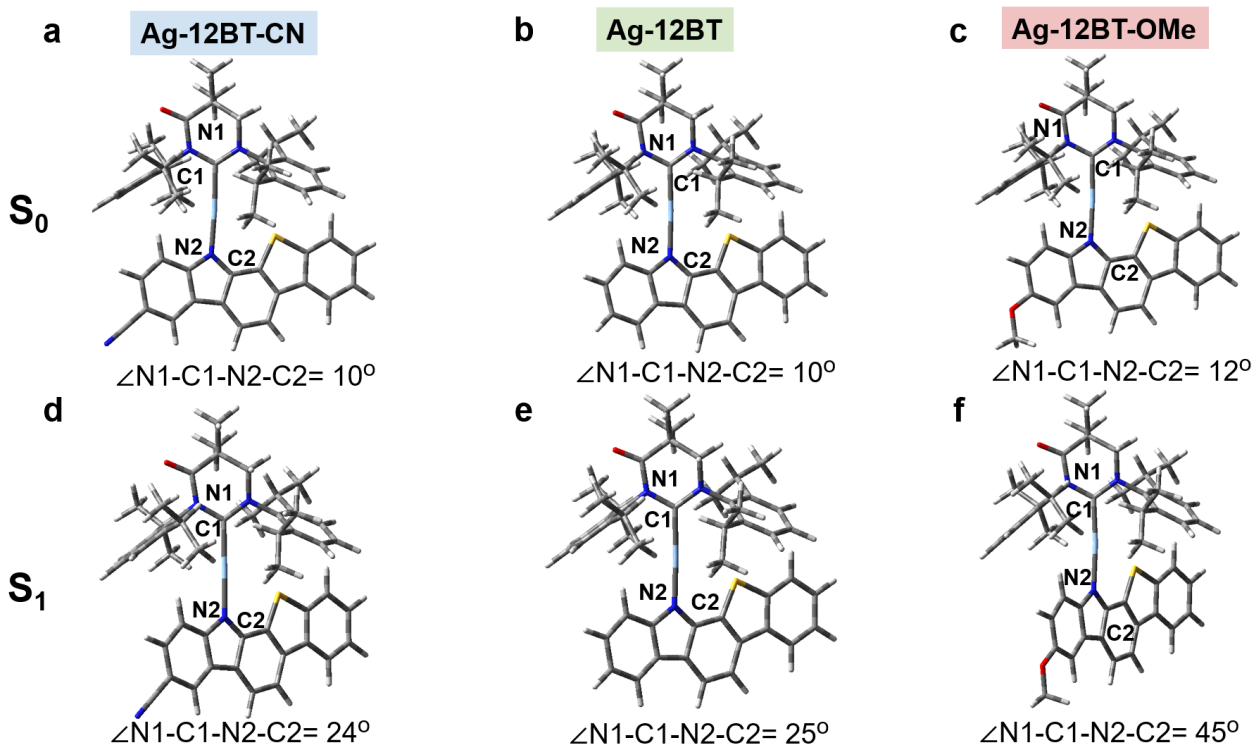

Fig. S4 Optimized S_0 and S_1 structures of Ag-12BT-CN, Ag-12BT, and Ag-12BT-OMe.

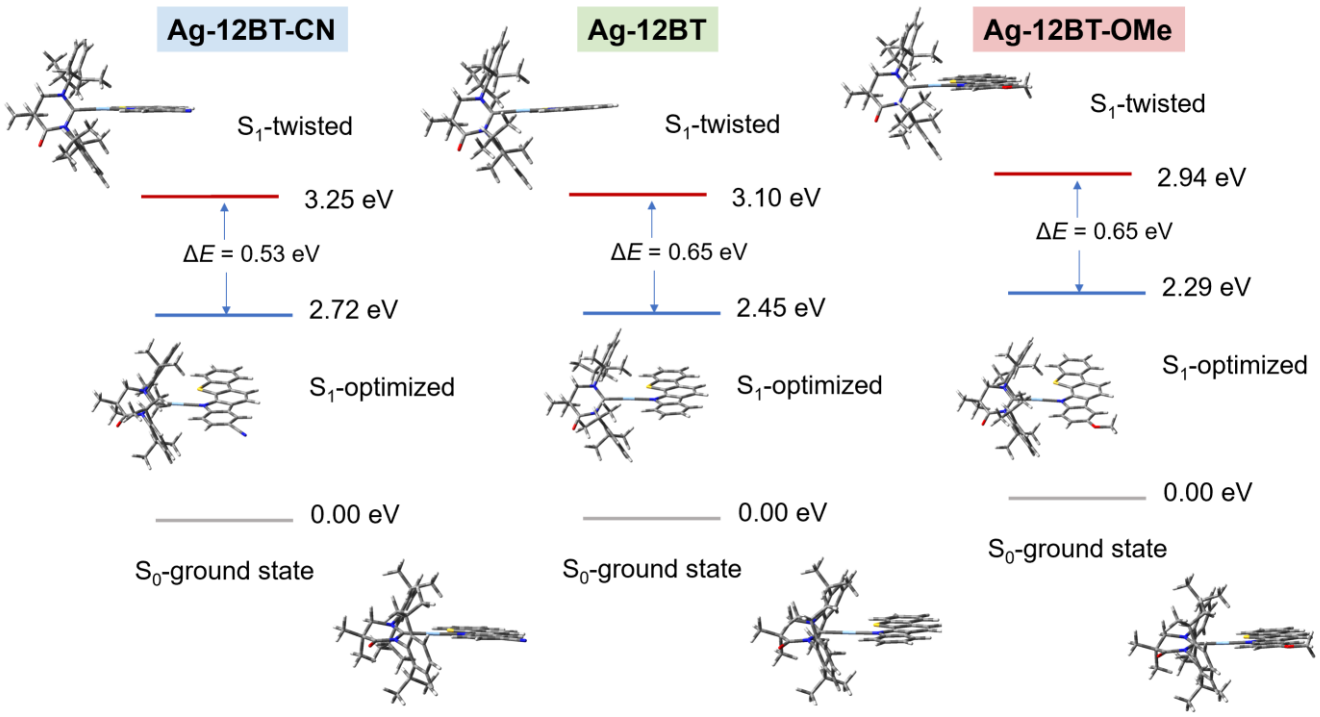

Fig. S5 Comparison of the energy levels of these Ag(I) emitters in optimized and orthogonal S_1 conformation.

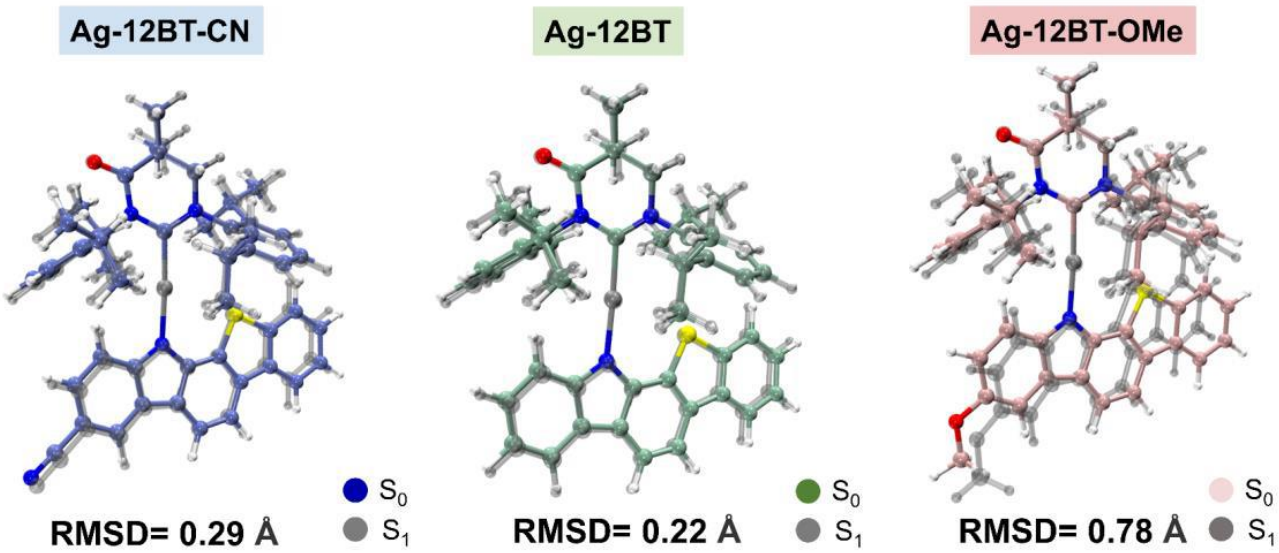

Fig. S6 The geometric deformation between the optimized S_0 and S_1 conformation of (a) Ag-12BT-CN, (b) Ag-12BT, and (c) Ag-12BT-OMe.

Table S2. Detail single crystal X-ray diffraction data of Ag-12BT-OMe.

Complex	Ag-12BT-OMe
Temperature	200 K
Moiety formula	$C_{49}H_{54}AgN_3O_2S{\cdot}2CH_2Cl_2$
Formula weight	1026.73
Crystal system	monoclinic
Space group	$P2_1/n$
a (Å):	15.0900(3)
b (Å):	14.1944(2)
c (Å):	24.1032(5)
alpha (deg.):	90
beta (deg.):	103.289(2)
gamma (deg.):	90
Volume (Å^3):	5024.51(17)
Z:	4
Dx (g/cm^3):	1.357
Mu (mm^{-1}):	5.882
F (000):	2128.0
Final R indices [I>2σ(I)]:	R_1 = 0.0759, wR_2 = 0.2012
R indices (all):	R_1 = 0.0825, wR_2 = 0.2092
Goodness-of-fit on F^2:	1.057

Table S3. Selected bond angles and lengths of Ag-12BT-OMe.

Structural parameters	Ag-12BT-OMe
C1–Ag–N3/°	171.85(17)
N1–C1–N3–C3/°	14.3 (2)
N1–C1–Ag/°	118.7(3)
N2–C1–Ag/°	123.2(3)
N1–C1–N2/°	117.2(4)
ΣCarbene/°	359.1(10)
C2–N3–Ag/°	124.1(3)
C3–N3–Ag/°	132.5(3)
C2–N3–C3/°	103.9(4)
ΣCarbazole/°	360.5(10)
C1–Ag/Å	2.103(5)
N3–Ag/ Å	2.082(4)

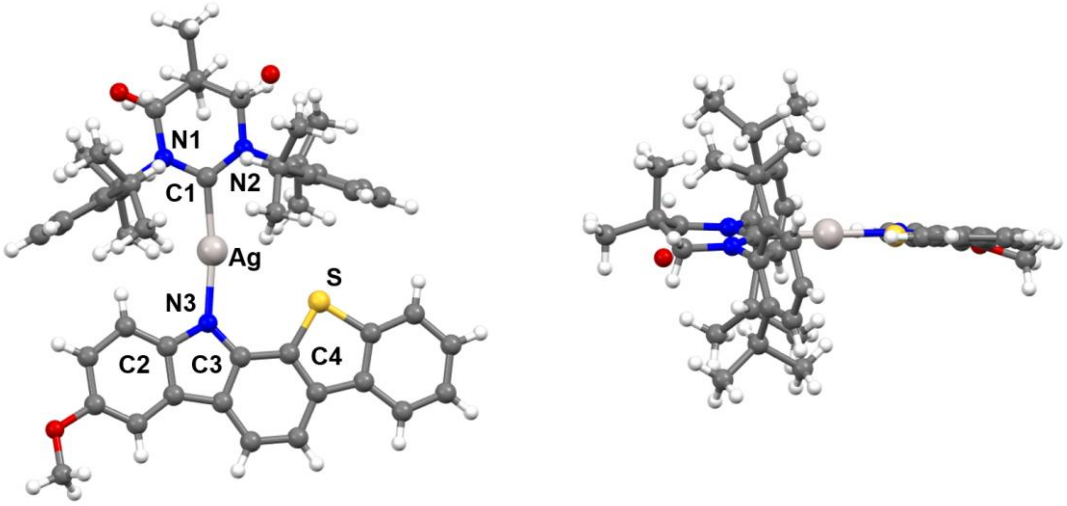

Fig. S7 Single-crystal structure of Ag-12BT-OMe.

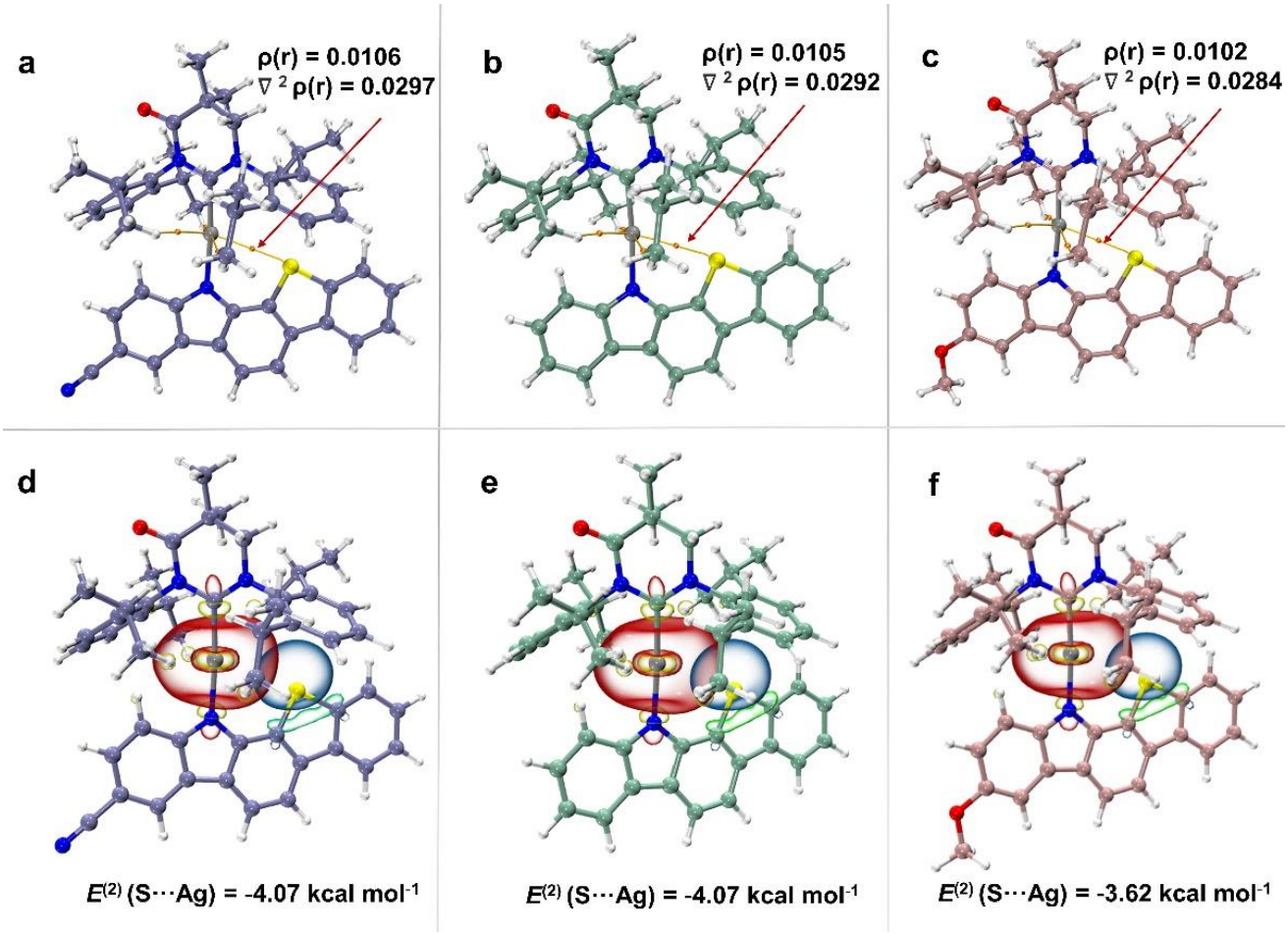

Fig. S8 AIM analysis of (a) Ag-12BT-CN, (b) Ag-12BT, and (c) Ag-12BT-OMe. NBO overlap between the n-orbital of S atoms and the s-orbital of the silver nucleus in (d) Ag-12BT-CN, (e) Ag-12BT, and (f) Ag-12BT-OMe. [Isovalue = 0.004 (electrons/bohr^3)$^{1/2}$]. $E^{(2)}$ represents stabilization energy taken from the corresponding interactions. The donor and acceptor NBOs are colored in blue/green and red/yellow, respectively.

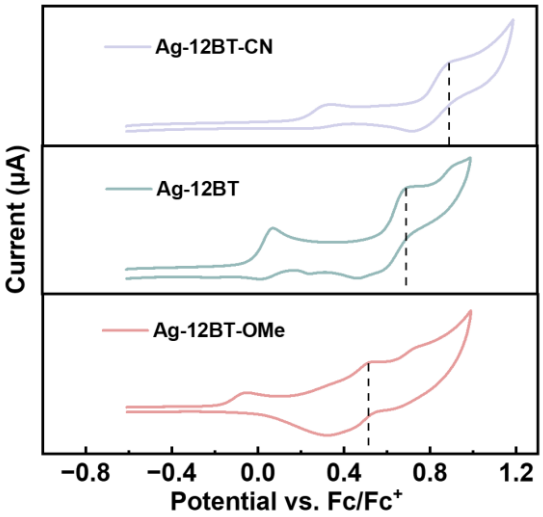

Fig. S9 Cyclic voltammograms of Ag-12BT-CN, Ag-12BT, and Ag-12BT-OMe in CH_2Cl_2 solutions.

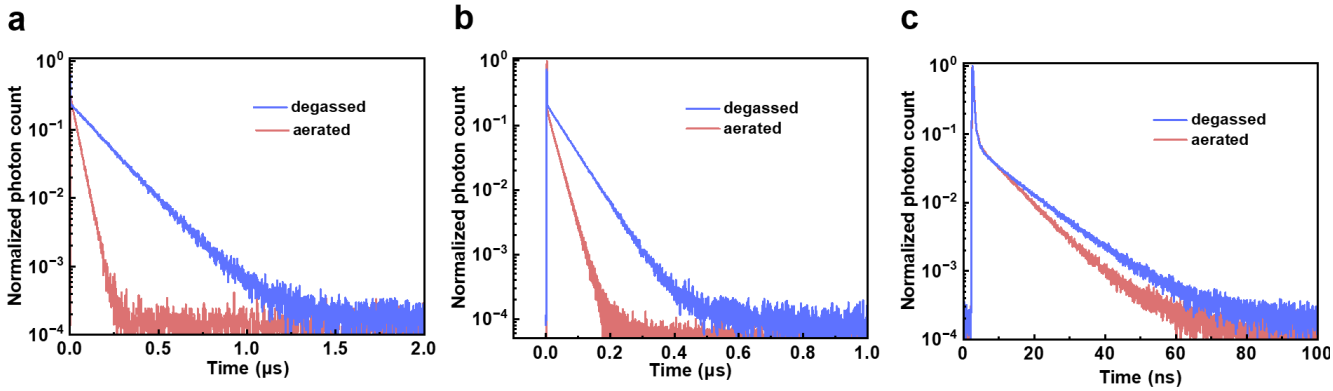

Fig. S10 Transient PL curves of (a) Ag-12BT-CN, (b) Ag-12BT, and (c) Ag-12BT-OMe under degassed and aerated conditions in toluene solutions (1×10^{-4} M, 300 K) following excitation at 375 nm.

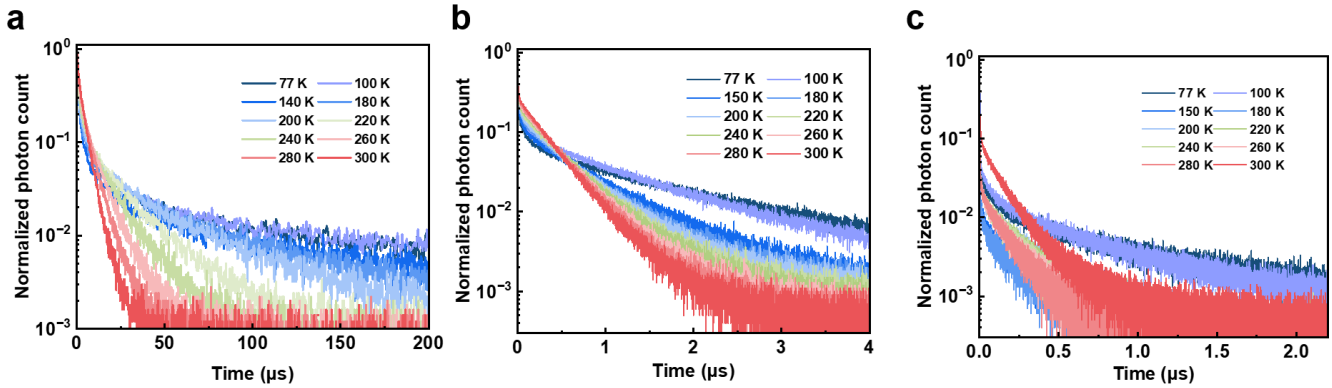

Fig. S11 Temperature-dependent transient PL spectra of (a) Ag-12BT-CN, (b) Ag-12BT, and (c) Ag-12BT-OMe in mCP-doped film with 30 wt% doping concentration following excitation at 375 nm.

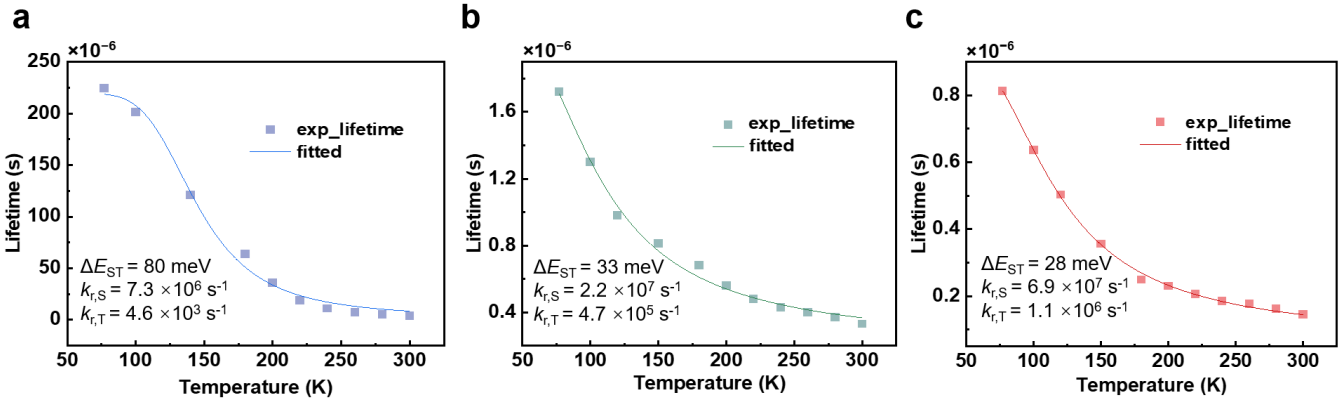

Fig. S12. Fit to temperature-dependent lifetimes (symbols) of (a) Ag-12BT-CN, (b) Ag-12BT, and (c) Ag-12BT-OMe to eq. S1 (curve) in mCP-doped film with 30 wt% doping concentration.

Table S4. Average observed decay lifetimes (τ_d) at different temperatures of Ag-12BT-CN, Ag-12BT, and Ag-12BT-OMe

T [K]	Ag-12BT-CN	Ag-12BT	Ag-12BT-OMe
77	224.5 μs (χ^2= 1.103)	1.72 μs (χ^2= 1.376)	0.81 μs (χ^2= 1.359)
100	201.3 μs (χ^2= 1.216)	1.30 μs (χ^2= 1.420)	0.64 μs (χ^2= 1.406)
120	174.4 μs (χ^2= 1.395)	0.98 μs (χ^2= 1.423)	0.50 μs (χ^2= 1.184)
160	78.6 μs (χ^2= 1.412)	0.81 μs (χ^2= 1.458)	0.356 μs (χ^2= 1.235)
180	63.7 μs (χ^2= 1.414)	0.68 μs (χ^2= 1.241)	0.249 μs (χ^2= 1.388)
200	36.0 μs (χ^2= 1.495)	0.56 μs (χ^2= 1.278)	0.230 μs (χ^2= 1.438)
220	18.6 μs (χ^2= 1.352)	0.48 μs (χ^2= 1.219)	0.205 μs (χ^2= 1.424)
240	11.0 μs (χ^2= 1.350)	0.43 μs (χ^2= 1.072)	0.185 μs (χ^2= 1.360)
260	7.44 μs (χ^2= 1.395)	0.40 μs (χ^2= 1.266)	0.176 μs (χ^2= 1.403)
280	5.38 μs (χ^2= 1.302)	0.37 μs (χ^2= 1.343)	0.162 μs (χ^2= 1.365)
300	3.90 μs (χ^2= 1.195)	0.33 μs (χ^2= 1.326)	0.144 μs (χ^2= 1.15d3)

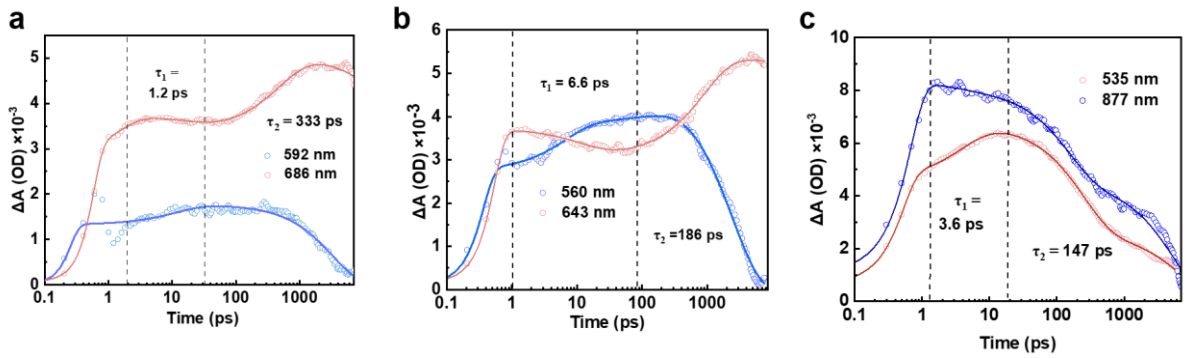

Fig. S13 Fs-transient kinetics of (a) Ag-12BT-CN at 592 and 686 nm, (b) Ag-12BT at 560 and 643 nm, and (c) Ag-12BT-OMe at 537 and 877 nm in 2 mg mL^{-1} chlorobenzene solutions, following excitation at 400 nm.

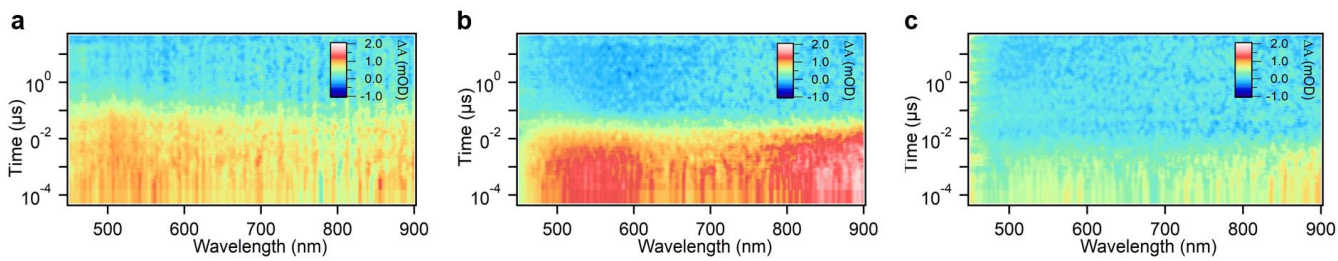

Fig. S14 Ns-TA evolution (a) Ag-12BT-CN at 517 nm, (b) Ag-12BT at 591 nm, and (c) Ag-12BT-OMe at 569 nm in 2 mg mL^{-1} chlorobenzene solutions, following excitation at 400 nm.

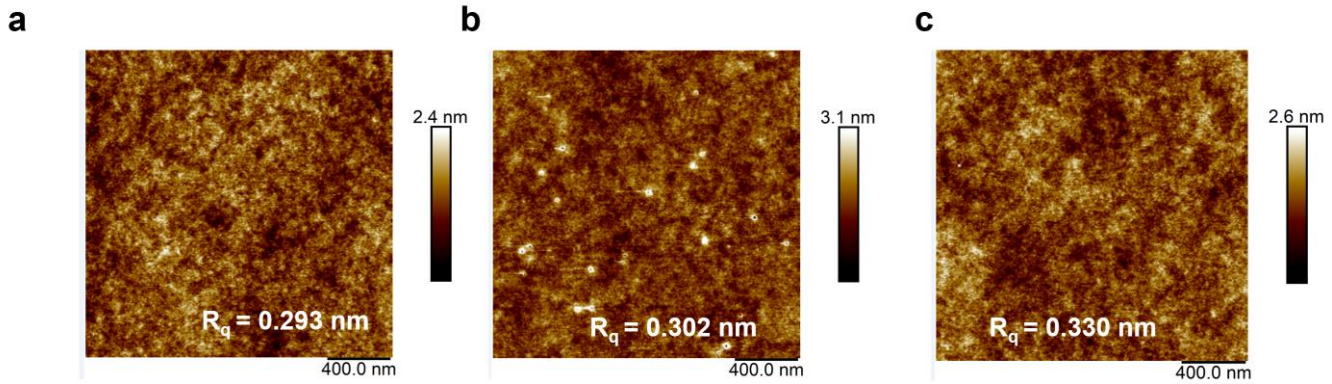

Fig. S15 Atom force microscopy (AFM) images of the doped films of (a) Ag-12BT-CN, (b) Ag-12BT, and (c) Ag-12BT-OMe in the mCP host.

Table S5. Summary of EL characteristics of the devices employing Ag(I) emitters (excluding Ag clusters with Au/Pt atom)

emitter	EL_{peak} [nm]	CE[a)] [cd A^{-1}]	PE[b)] [lm W^{-1}]	EQE[c)] [%]	Φ_{PL} [%]	Ref.
Ag-1	585	38.1	29.9	14.7	72	[9]
Ag-2	~570	23.1	9.2	8.8	62	[10]
Ag-3	542	--	--	4.6	74	[11]
Ag-4	540	--	--	13.7	54	[11]
Ag-12BT-CN	512	35.0	31.4	12.8	60	This work
Ag-12BT	528	48.7	43.7	16.2	72	This work
Ag-12BT-OMe	558	12.8	6.5	4.4	23	This work

Maximum values of [a)] current efficiency, [b)] power efficiency, and [c)] external quantum efficiency.

Table S6. Summary of EL characteristics of the Ag-12BT based devices with different doping concentrations

Doping concentration	V_{on}[a)] [V]	CE[b)] [cd A^{-1}]	PE[c)] [lm W^{-1}]	EQE[d)] [%]	EL_{peak} [nm]
20 wt%	3.8	42.2	27.2	14.4	526
30 wt%	3.2	48.7	43.7	16.2	528
40 wt%	3.8	37.3	25.9	12.4	534
50 wt%	3.2	36.7	28.2	12.2	533

[a)] The turn-on voltage recorded at a luminance of 1 cd m^{-2}. Maximum values of [b)] current efficiency, [c)] power efficiency, and [d)] external quantum efficiency.

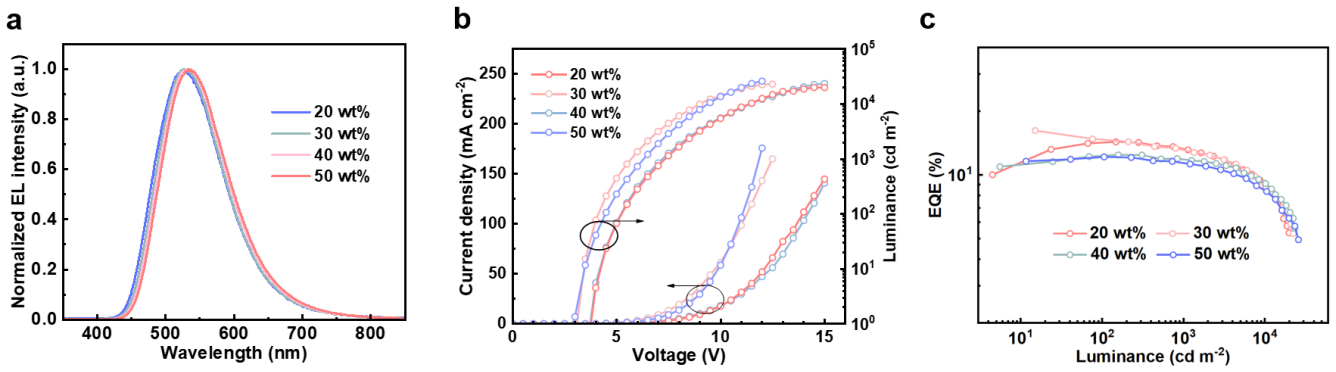

Fig. S16 (a) Normalized EL spectra (b) Current density-voltage-luminance curves (c) External quantum efficiency as a function of luminance for the devices based on Ag-12BT emitter with different doping concentrations.

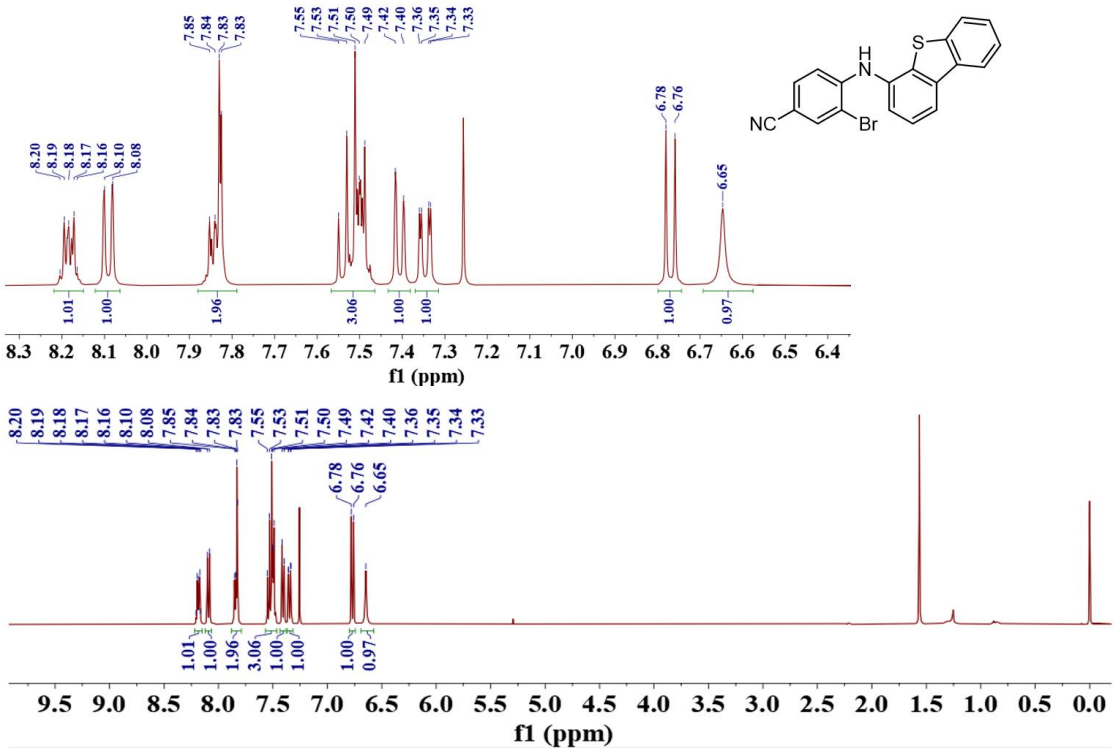

Fig. S17 ^{1}H NMR spectrum of 3-bromo-4-(dibenzo[b,d]thiophen-4-ylamino)benzonitrile (400 MHz, CD_2Cl_2, 300 K).

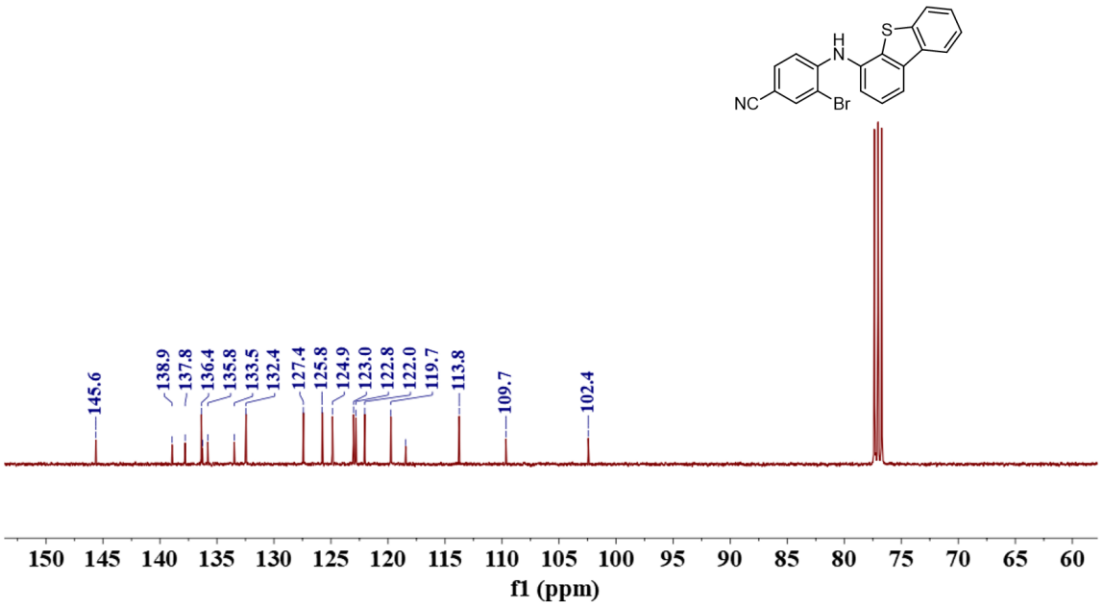

Fig. S18 ^{13}C NMR spectrum of 3-bromo-4-(dibenzo[b,d]thiophen-4-ylamino)benzonitrile (101 MHz, CD_2Cl_2, 300 K).

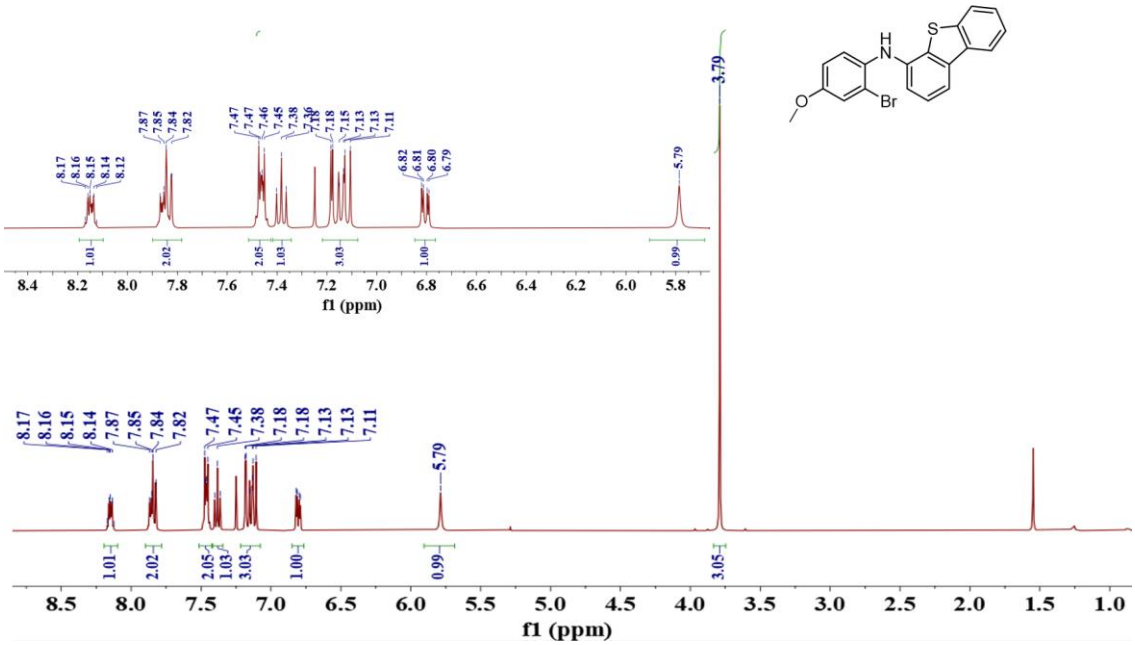

Fig. S19 ^{1}H NMR spectrum of *N*-(2-bromo-4-methoxyphenyl)dibenzo[b,d]thiophen-4-amine (400 MHz, CD_2Cl_2, 300 K).

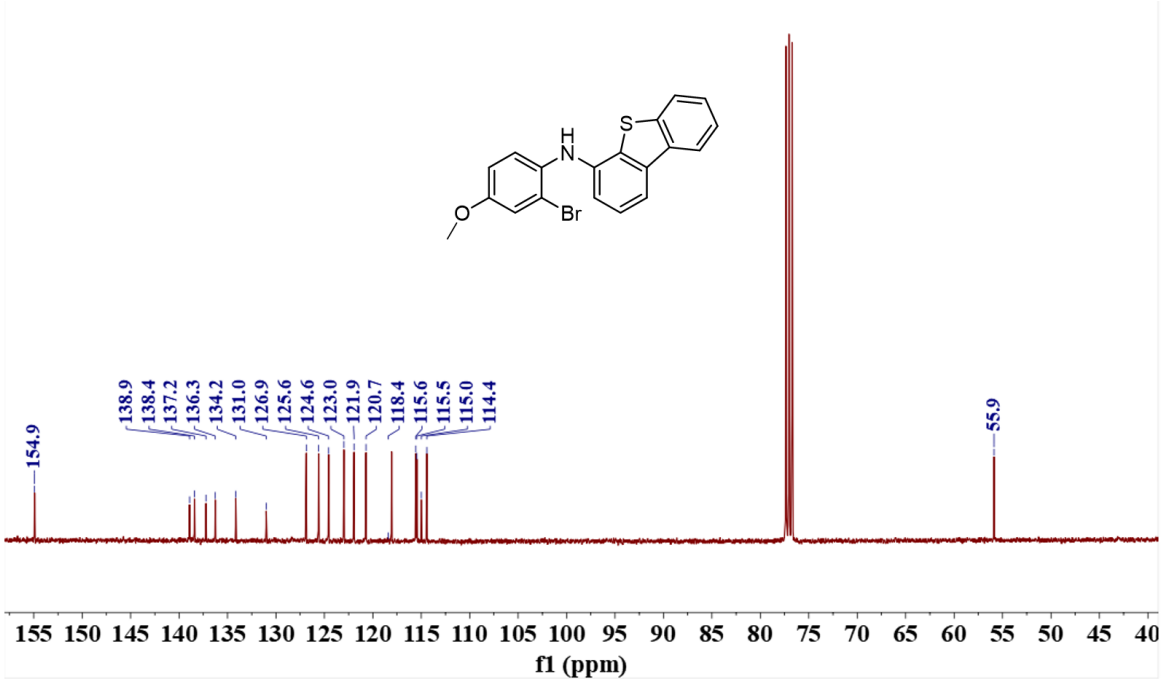

Fig. S20 ^{13}C NMR spectrum of *N*-(2-bromo-4-methoxyphenyl)dibenzo[b,d]thiophen-4-amine (101 MHz, CD_2Cl_2, 300 K).

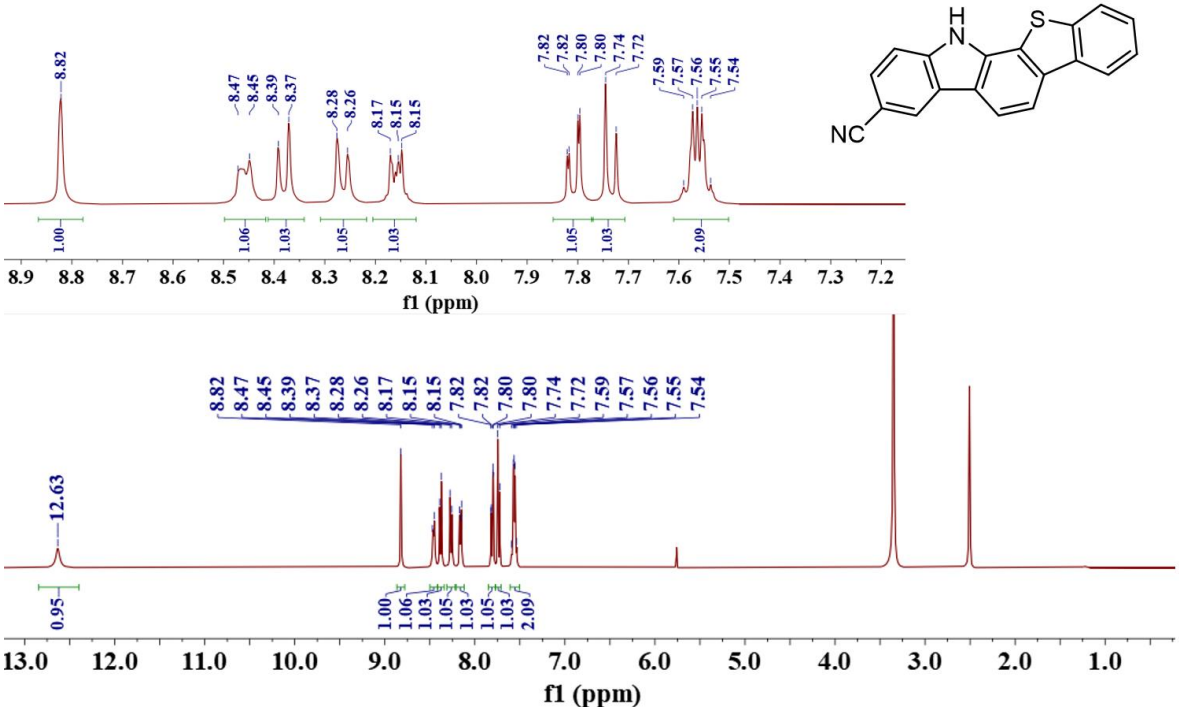

Fig. S21 ^{1}H NMR spectrum of 12BT-CN (400 MHz, DMSO-d_6, 300 K).

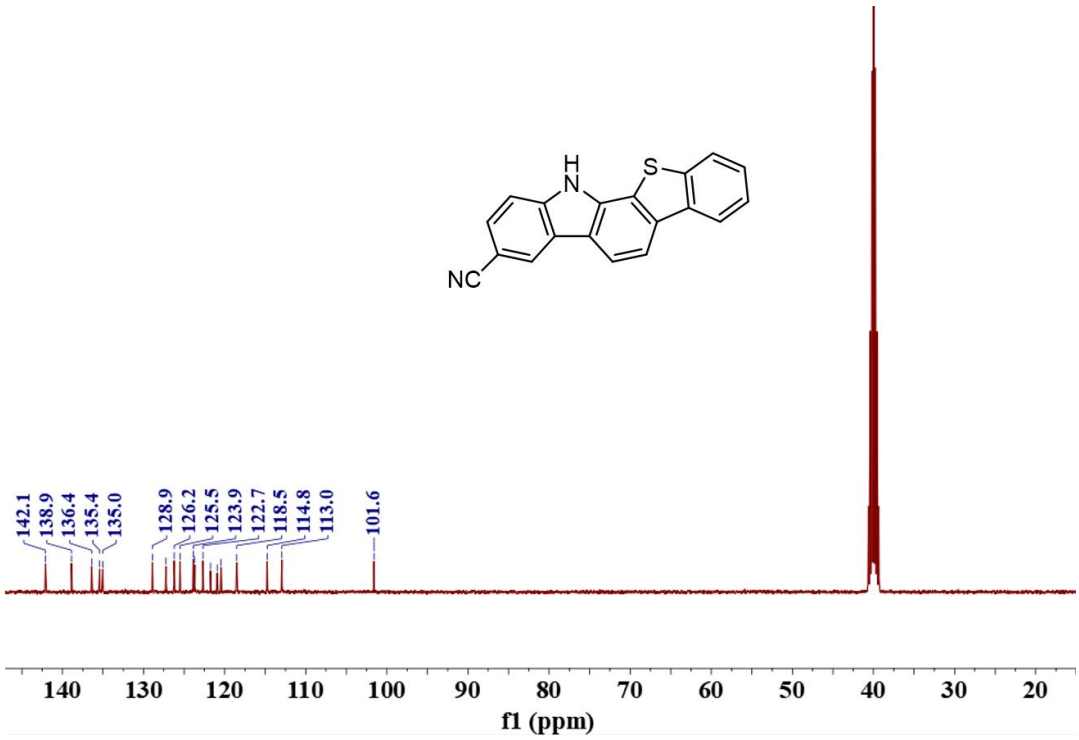

Fig. S22 ^{13}C NMR spectrum of 12BT-CN (101 MHz, DMSO-d_6, 300 K).

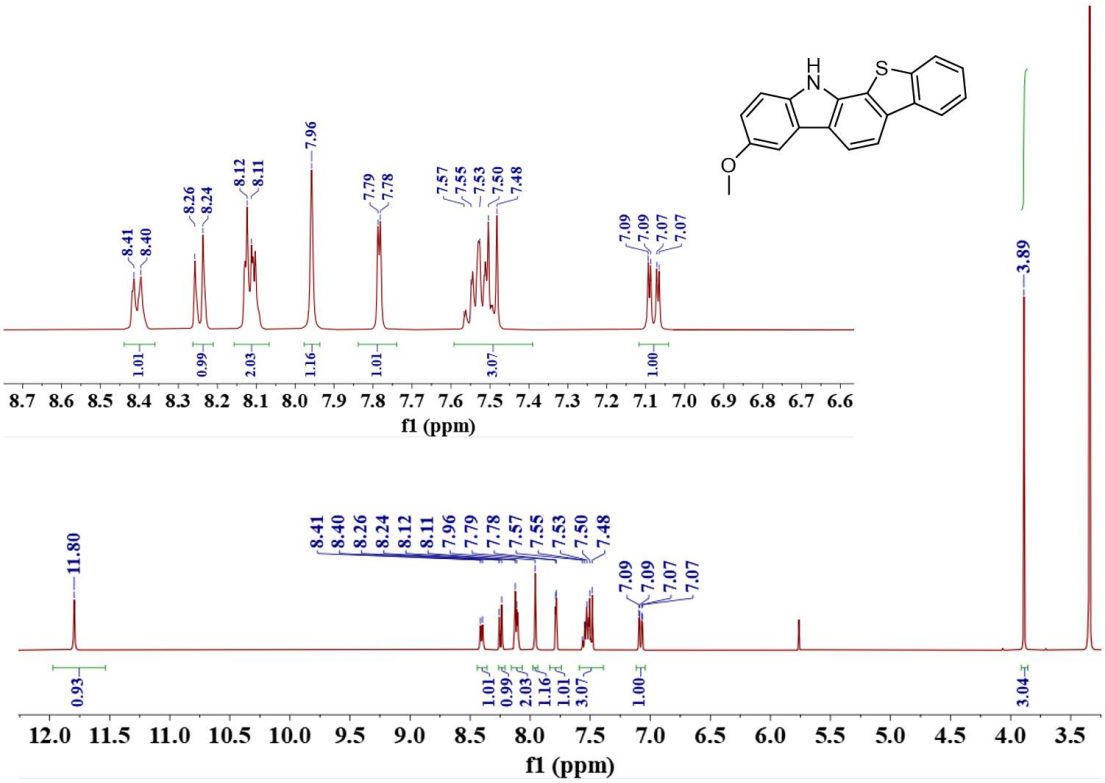

Fig. S23 ^{1}H NMR spectrum of 12BT-OMe (400 MHz, DMSO-d_6, 300 K).

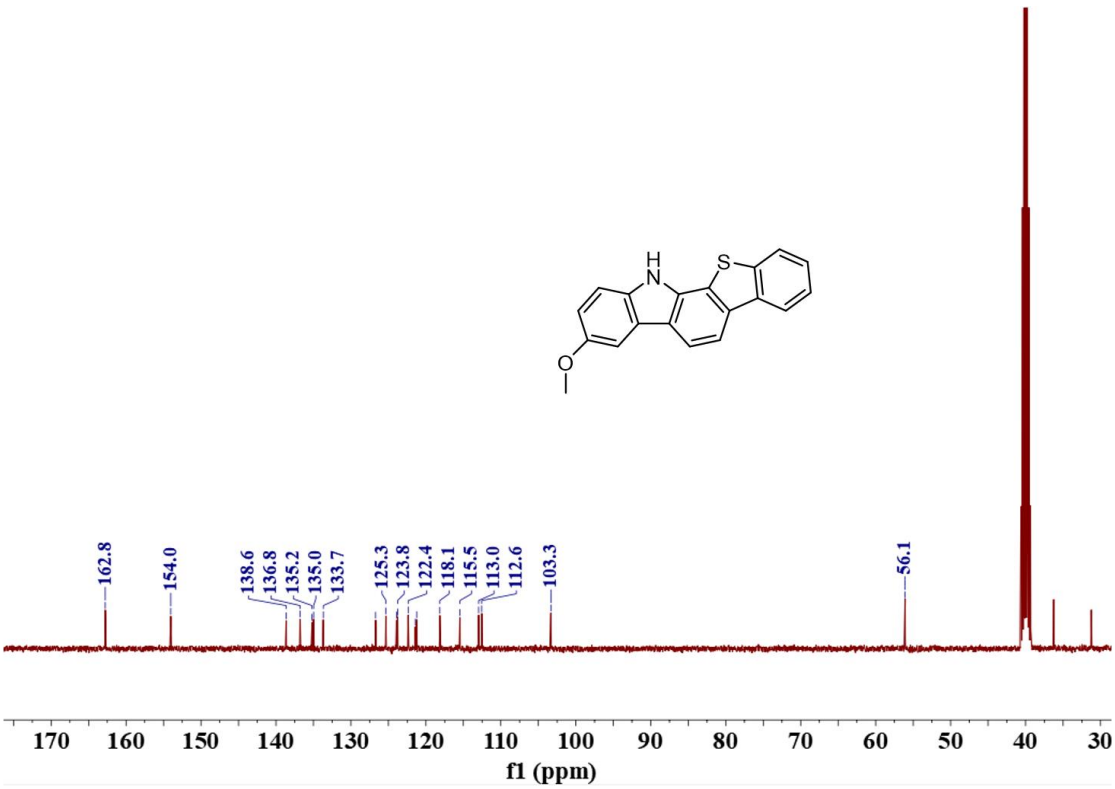

Fig. S24 ^{13}C NMR spectrum of 12BT-CN (101 MHz, DMSO-d_6, 300 K).

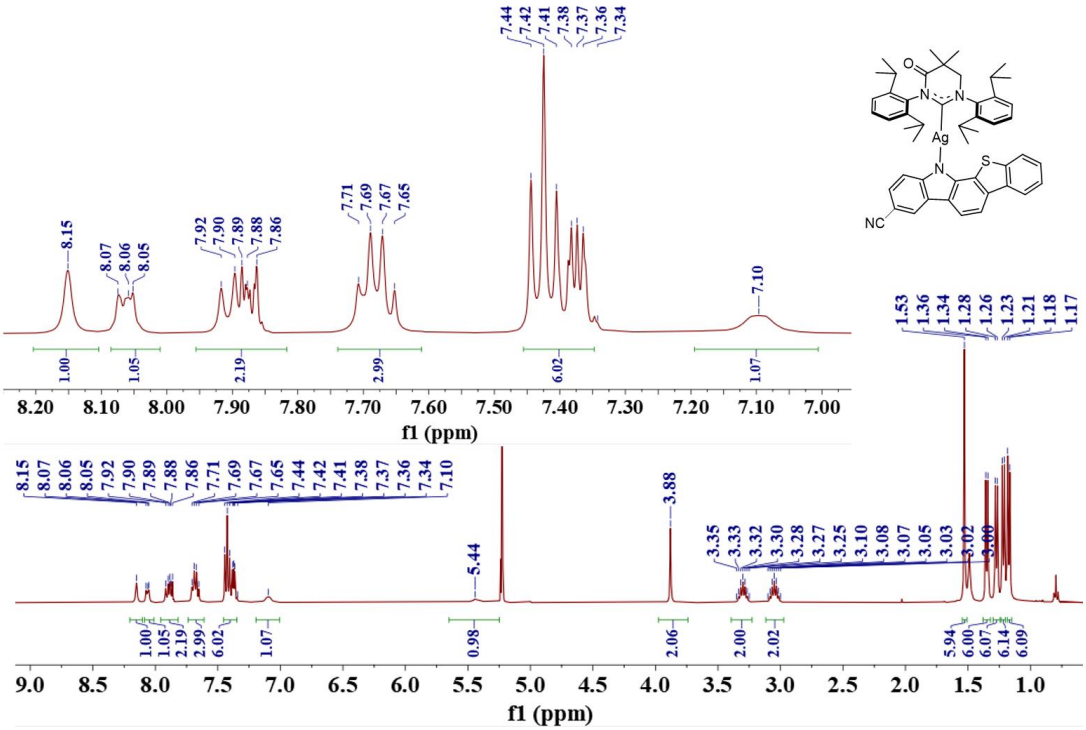

Fig. S25 ^{1}H NMR spectrum of Ag-12BT-CN (400 MHz, CD_2Cl_2, 300 K).

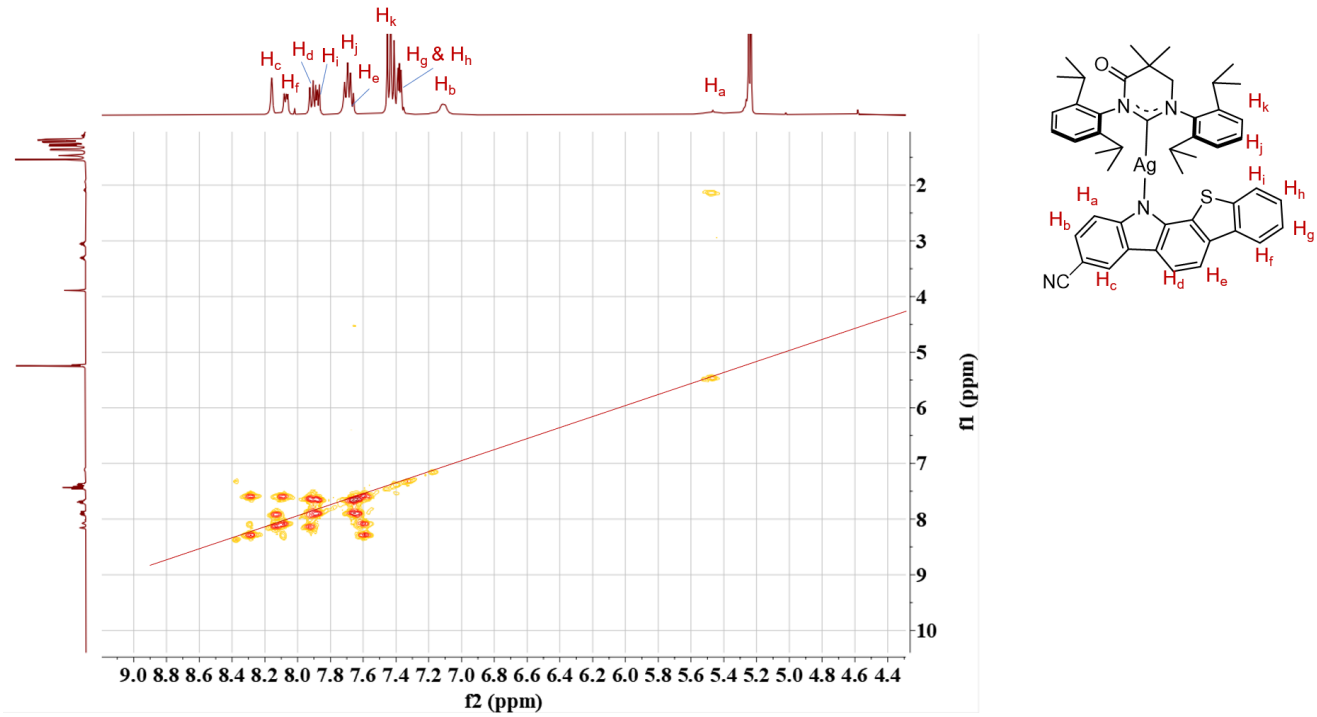

Fig. S26 ^{1}H-^{1}H COSY spectrum of Ag-12BT-CN (400 MHz, CD_2Cl_2, 300 K).

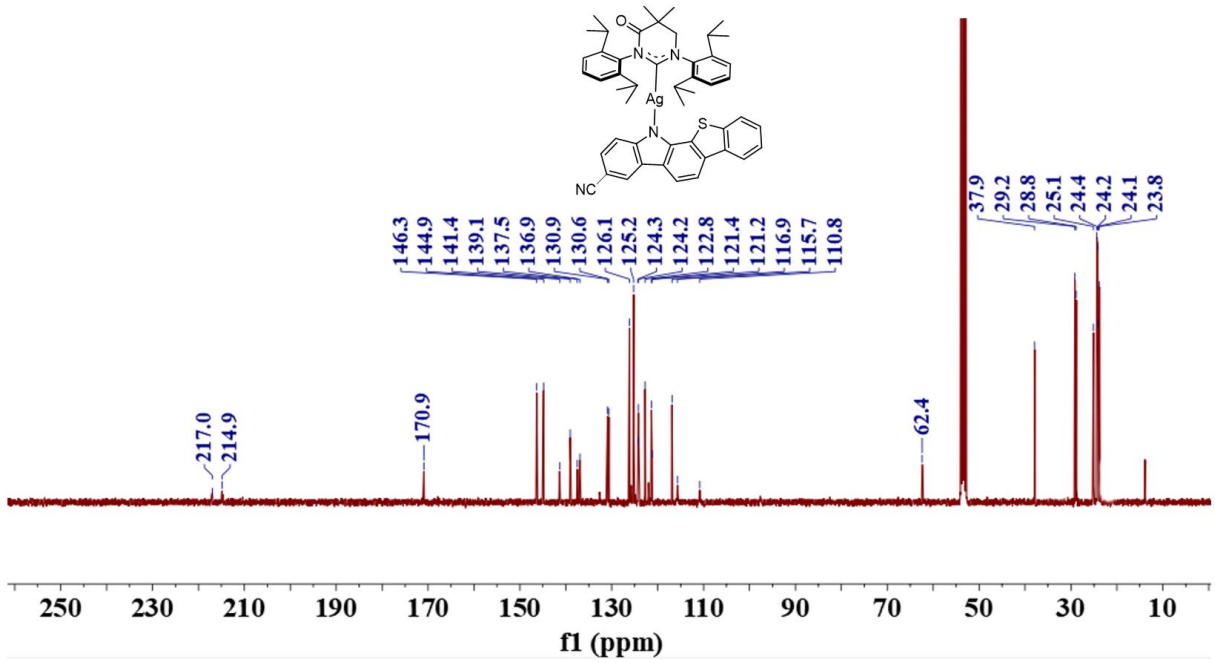

Fig. S27 ^{13}C NMR spectrum of Ag-12BT-CN (101 MHz, CD_2Cl_2, 300 K).

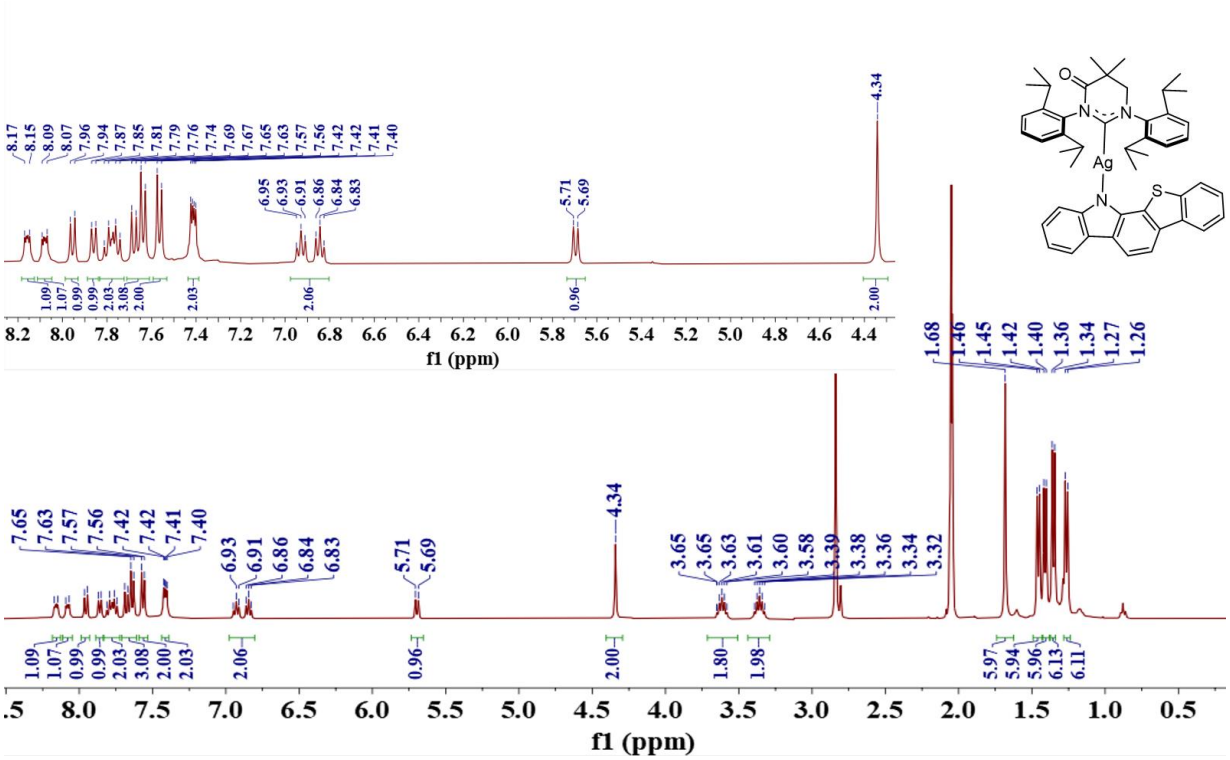

Fig. S28 ^{1}H NMR spectrum of Ag-12BT (400 MHz, Acetone-d_6, 300 K).

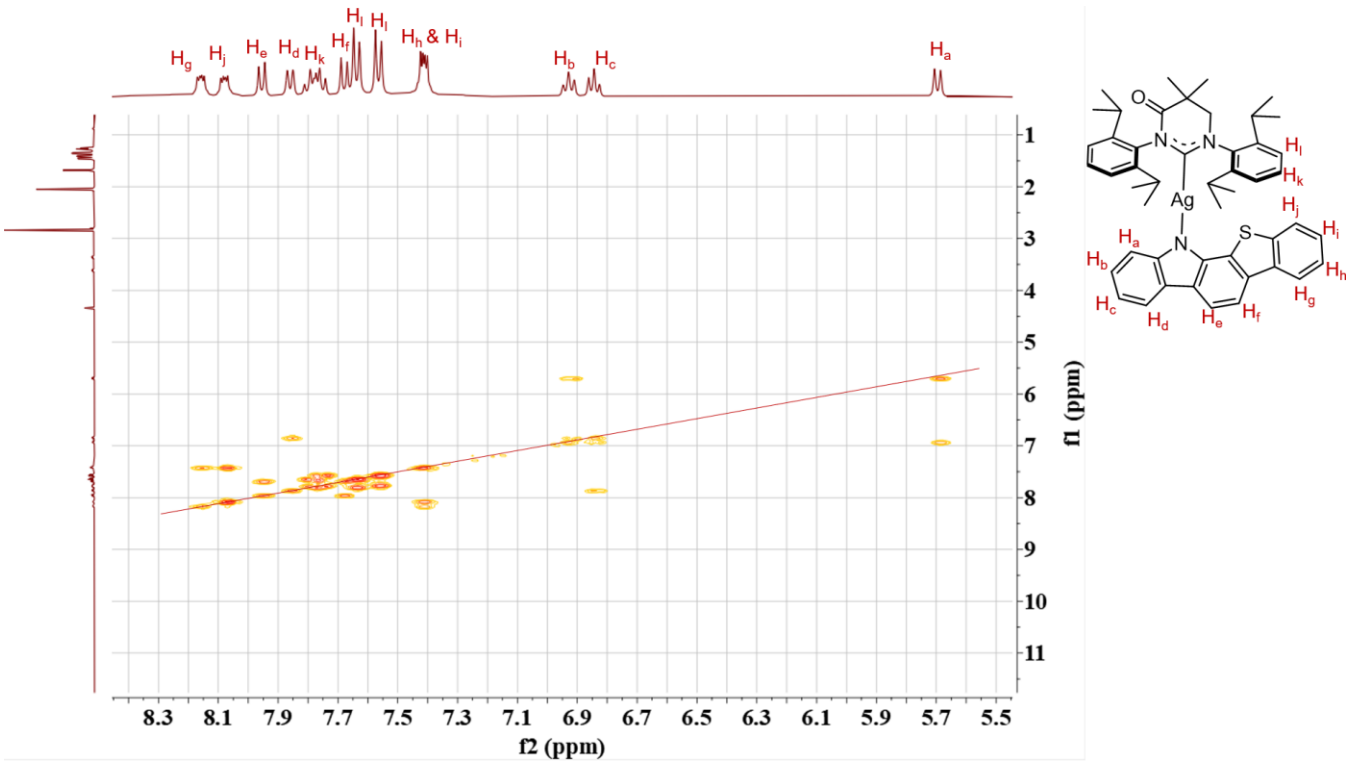

Fig. S29 ^{1}H-^{1}H COSY spectrum of Ag-12BT (400 MHz, Acetone-d_6, 300 K).

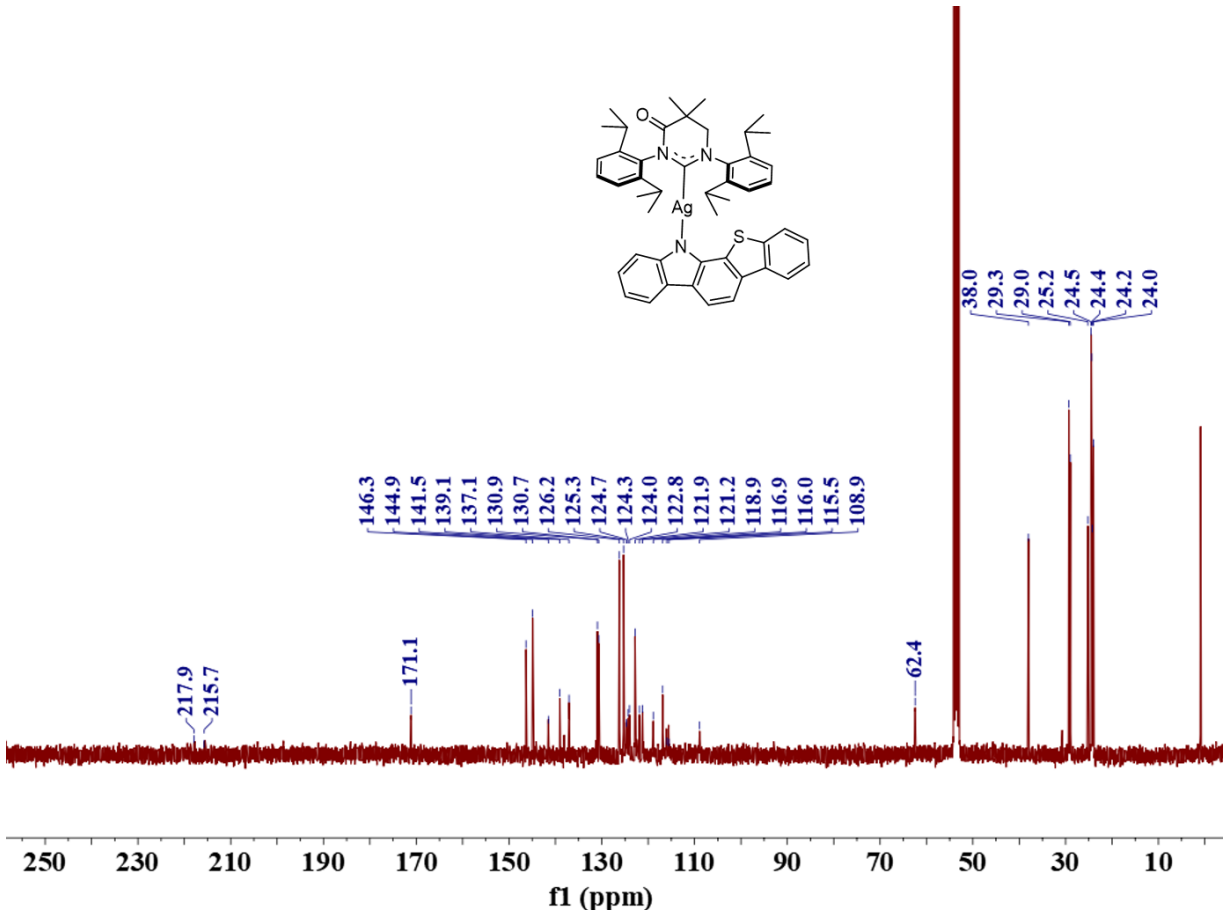

Fig. S30 ^{13}C NMR spectrum of Ag-12BT (101 MHz, CD_2Cl_2, 300 K).

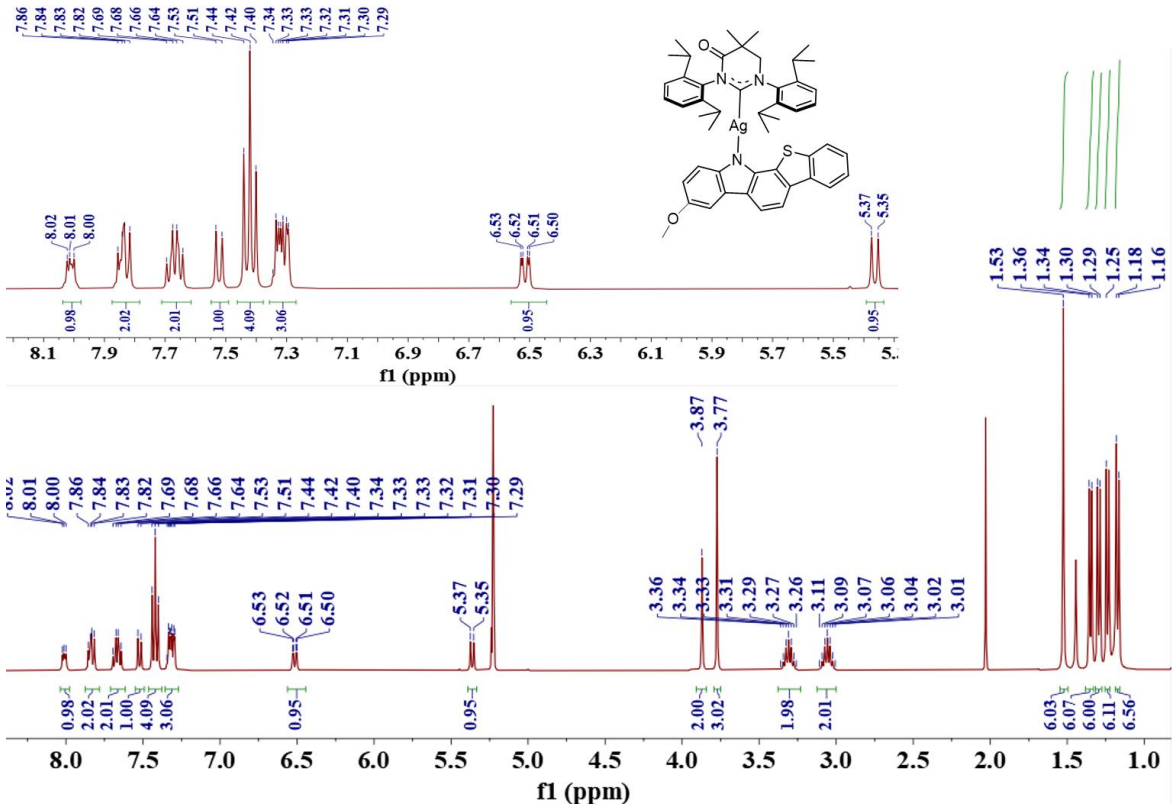

Fig. S31 ^{1}H NMR spectrum of Ag-12BT-OMe (400 MHz, CD_2Cl_2, 300 K).

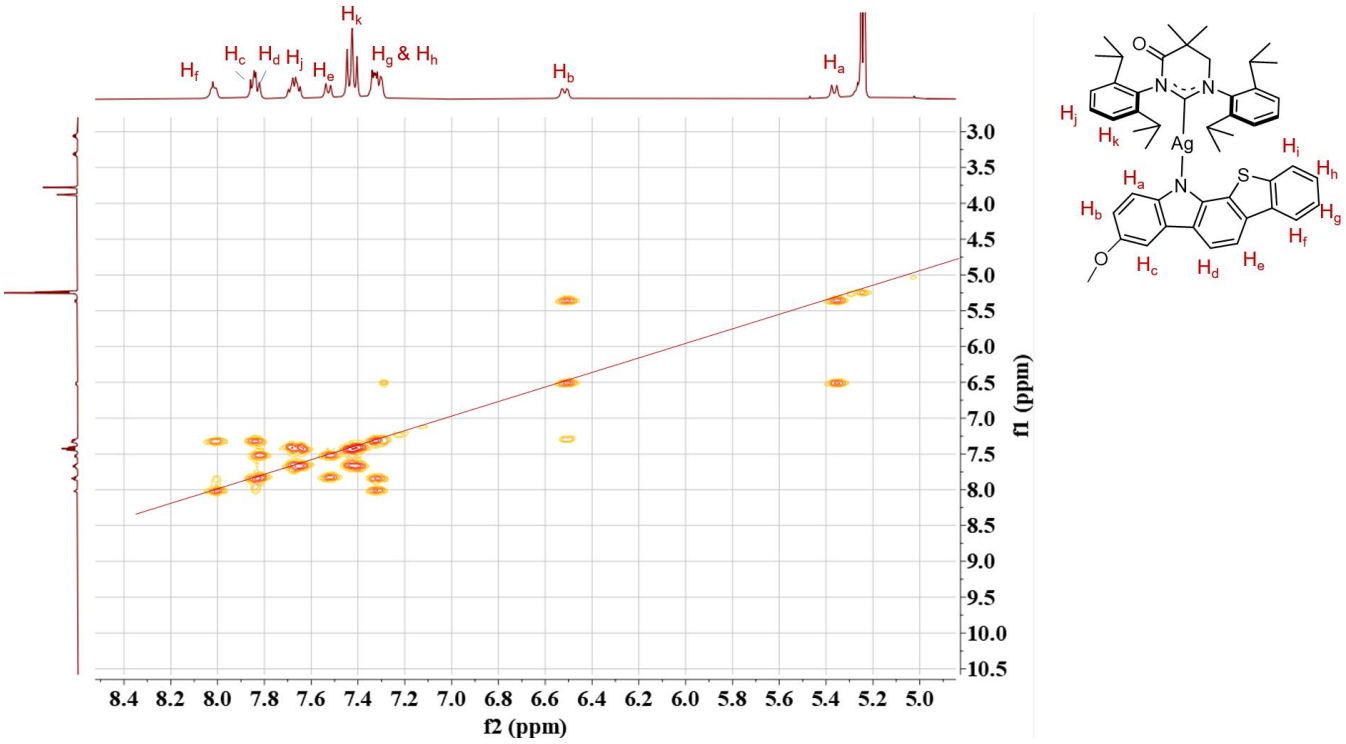

Fig. S32 ^{1}H-^{1}H COSY spectrum of Ag-12BT-OMe (400 MHz, CD_2Cl_2, 300 K).

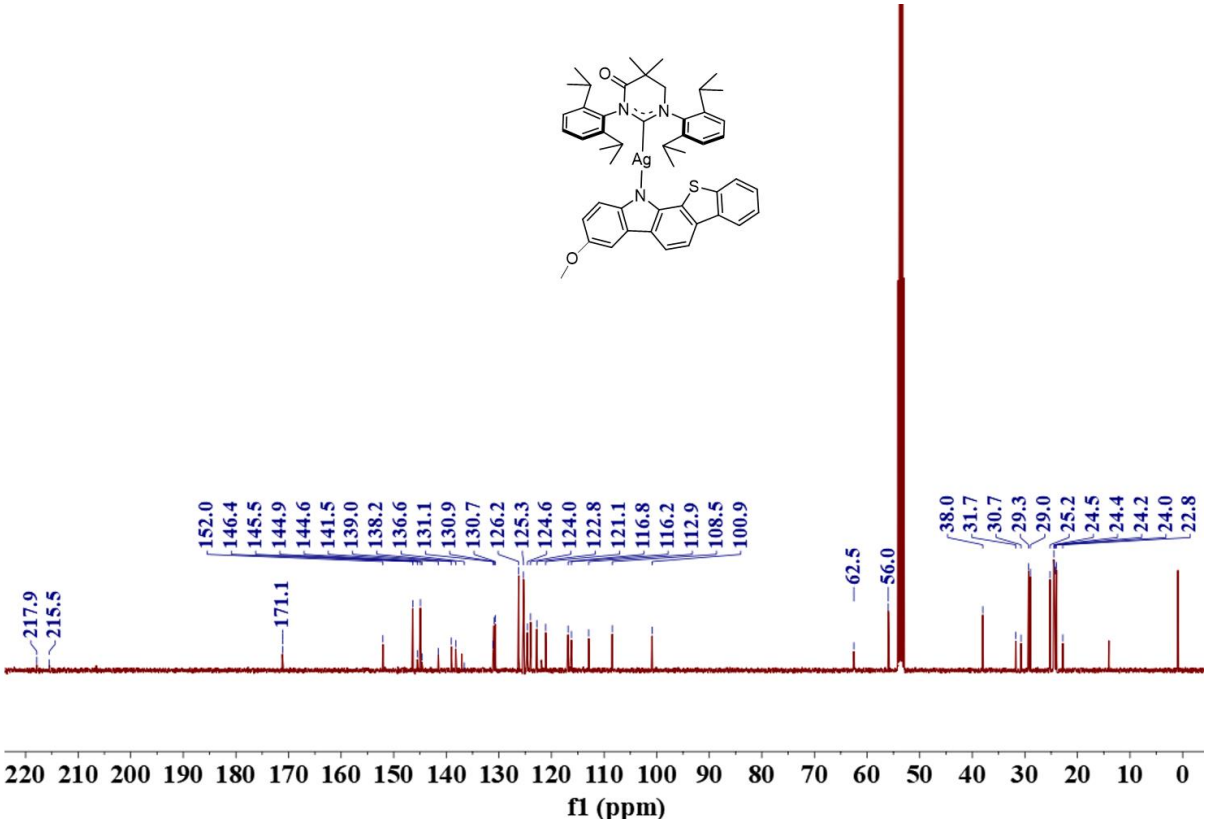

Fig. S33 ^{13}C NMR spectrum of Ag-12BT-OMe (101 MHz, CD_2Cl_2, 300 K).

References

1 Agilent Technologies, CrysAlisPRO, Version 1.171.36.28, 2013.

2 O. V. Dolomanov, L. J. Bourhis, R. J. Gildea, J. A. K. Howard, H. and J. Puschmann, *J. Appl. Cryst.* 2009, **42**, 339.

3 D. Kratzert, J. J. Holstein and I. Krossing, *J. Appl. Cryst.* 2015, **48**, 933–938.

4 Y. Zhao and D. G. Truhlar, *J. Chem. Phys.* 2006, **125**, 194101.

5 A. Ying, 2024, CCDC Experimental Crystal Structure Determination: 2305500, DOI: 10.5517/ccdc.csd.cc2hd1zy.

6 S. Grimme, J. Antony, S. Ehrlich and H. Krieg, *J. Chem. Phys.* 2010, **132***,* 154104.

7 T. Lu and F. Chen, *J. Comput. Chem.* 2012, **33**, 580–592.

8 R. Hamze, S. Shi, S. C. Kapper, D. S. Muthiah Ravinson, L. Estergreen, M. C. Jung, A. C. Tadle, R. Haiges, P. I. Djurovich, J. L. Peltier, R. Jazzar, G. Bertrand, S. E. Bradforth and M. E. Thompson, *J. Am. Chem. Soc.* 2019, **141**, 8616–8626.

9 Z. Jiao, M. Yang, J.-Y. Wang, Y.-Z. Huang, P. Xie and Z.-N. Chen, *J. Mater. Chem. C* 2021, **9**, 5528–5534.

10 T. Teng, K. Li, G. Cheng, Y. Wang, J. Wang, J. Li, C. Zhou, H. Liu, T. Zou, J. Xiong, C. Wu, H.-X. Zhang, C.-M. Che and C. Yang, *Inorg. Chem.* 2020, **59**, 12122–12131.

11 A. S. Romanov, S. T. E. Jones, L. Yang, P. J. Conaghan, D. Di, M. Linnolahti, D. Credgington and M. Bochmann, *Adv. Opt. Mater.* 2018, **6**, 1801347.